



Defence Research and
Development Canada

Recherche et développement
pour la défense Canada



Ship detection using RADARSAT-2 Fine Quad Mode and simulated compact polarimetry data

Chen Liu, Paris W. Vachon, Ryan A. English and Nicholas Sandirasegaram

Defence R&D Canada – Ottawa

Technical Memorandum
DRDC Ottawa TM 2009-285
February 2010

Canada

Ship detection using RADARSAT-2 Fine Quad Mode and simulated compact polarimetry data

Chen Liu, Paris W. Vachon, Ryan A. English and Nicholas Sandirasegaram

DRDC Ottawa

Defence R&D Canada – Ottawa

Technical Memorandum

DRDC Ottawa TM 2009-285

February 2010

Principal Author

Original signed by Chen Liu

Chen Liu

Defence Scientist

Approved by

Original signed by Caroline Wilcox

Caroline Wilcox

Head, Radar Applications and Space Technologies Section

Approved for release by

Original signed by Brian Eatock

Brian Eatock

Chair, Document Review Panel

© Her Majesty the Queen in Right of Canada, as represented by the Minister of National Defence, 2010

© Sa Majesté la Reine (en droit du Canada), telle que représentée par le ministre de la Défense nationale, 2010

Abstract

This Technical Memorandum presents an evaluation baseline for ship detection employing RADARSAT-2 Fine Quad (FQ) Mode imagery and an initial investigation of the potential performance for data obtained by a compact polarimetry (CP) SAR system. A CP SAR system with circular polarization on transmission and two orthogonal linear polarizations on receive was simulated using RADARSAT-2 FQ data. Polarimetric SAR (PolSAR) ship detection algorithms were applied to both the FQ and simulated CP data. From statistical decision theory, the likelihood ratio test with Neyman-Pearson criterion was used to define a decision variable.

FQ, dual polarization (including simulated CP, and horizontal polarization on transmit and horizontal and vertical polarizations on receive (HH + HV) with amplitude only), and single polarization (HH) images of known ships were considered. In this study, the smallest detected ship had a length of 18 m. The results demonstrate that a quad polarization system provides the best ship detection performance in this application as compared to single and dual polarization SAR systems. The results also demonstrate that a CP system provides better performance than a conventional dual polarization system and in turn than a single polarization system. It is important to note that CP, dual polarization and single polarization systems have a swath width that is twice as wide as that of a PolSAR having the same resolution.

Detection performance was characterized by calculating receiver operating characteristics for RADARSAT-2 FQ data and simulated CP data to quantify the trade-off between the probability of missed detection and the probability of false alarm. SAR detections were validated by using automatic identification system (AIS) data.

In further studies, detection algorithms based on the likelihood ratio test have been optimized and the decision variable defined using the likelihood ratio test has been input into a K-distribution constant false alarm rate (KCFAR) detector as the required image. The KCFAR PolSAR (KCFAR_Quad) detector found all targets for which AIS data were available, and also additional targets. Results show that this detector is capable of detecting smaller targets than those for a single polarization system.

Résumé

Le présent mémoire technique porte sur une référence d'évaluation pour la détection des navires au moyen d'imagerie en mode à polarisation en quadrature (quad-pol) fin de RADARSAT-2 ainsi que sur une première étude du rendement potentiel d'un système de radar à synthèse d'ouverture (SAR) à polarimétrie compacte (CP). Un système de SAR CP où l'émission se fait avec une polarisation circulaire et la réception avec deux polarisations rectilignes orthogonales a été simulé au moyen de données du mode polarisation en quadrature fin (FQ) de RADARSAT-2. Des algorithmes de détection de navires par SAR polarimétrique (PolSAR) ont été appliqués aux données FQ et aux données CP simulées. Le test de rapport de vraisemblance avec critère de Neyman-Pearson, issu de la théorie statistique de la décision, a servi à définir une variable de décision.

L'étude a porté sur des images de navires connus obtenues en mode FQ, en mode polarisation double (y compris en mode CP simulée et en mode à émission en polarisation horizontale et à réception en polarisation verticale (HH + HV) avec amplitude seulement) et en mode polarisation simple (HH). Dans la présente étude, le plus petit navire détecté avait une longueur de 18 m. Les résultats montrent qu'un système à polarisation en quadrature offre le meilleur rendement de détection des navires dans cette application que les systèmes SAR à polarisation simple ou double. Les résultats démontrent également qu'un système CP permet d'obtenir un meilleur rendement qu'un système à polarisation double classique, qui offre à son tour un rendement supérieur à celui d'un système à polarisation simple. Il est important de noter que les systèmes CP et les systèmes à polarisation simple ou double ont une bande au sol deux fois plus large qu'un système PolSAR de même résolution.

Le rendement de détection a été caractérisé en calculant la courbe ROC (*Receiver Operating Characteristics*) à partir des données FQ de RADARSAT-2 et des données CP simulées afin de quantifier le compromis entre la probabilité de détection manquée et la probabilité de fausse alarme. Les détections SAR ont été validées au moyen des données du système d'identification automatique (AIS).

Au cours d'études subséquentes, des algorithmes de détection fondés sur le test de rapport de vraisemblances ont été optimisés, et la variable de décision définie au moyen du test de rapport de vraisemblances a été entrée dans un détecteur à taux de fausse alarme constant à distribution K (KCFAR) en tant qu'image requise. Le détecteur KCFAR PolSAR (KCFAR_Quad) a détecté toutes les cibles pour lesquelles des données AIS étaient disponibles, ainsi que d'autres cibles. Les résultats montrent que ce détecteur peut détecter des cibles beaucoup plus petites qu'un système à polarisation simple.

Executive summary

Ship detection using RADARSAT-2 Fine Quad Mode and simulated compact polarimetry data

Chen Liu; Paris W. Vachon; Ryan A. English; Nicholas Sandirasegaram

DRDC Ottawa TM 2009-285; Defence R&D Canada – Ottawa; February 2010.

Introduction: RADARSAT-2 capabilities include polarimetric synthetic aperture radar (PolSAR) modes. Improved ship detection using PolSAR data over single channel data has been previously demonstrated using airborne PolSAR data. In this Technical Memorandum, the application of PolSAR ship detection algorithms developed using airborne data to RADARSAT-2 Fine Quad (FQ) Mode data is evaluated.

Compact polarimetric (CP) SAR is an approach to dual polarization SAR. One form is hybrid-polarity in which a circularly polarized wave is transmitted and two orthogonal, mutually-coherent linearly polarized waves are received. CP SAR has a wider swath width than quad polarization systems of the same resolution. As described in this report, hybrid-polarity SAR using RADARSAT-2 FQ data is simulated. PolSAR ship detection algorithms then were applied to the simulated CP SAR data.

The dual polarization HH + HV with amplitude only and single polarization (HH) data were extracted from the RADARSAT-2 FQ data.

Based on statistical decision theory, the likelihood ratio test with Neyman-Pearson criterion was used to define a decision variable. Detection performance was characterized by calculating receiver operating characteristics for RADARSAT-2 FQ data and simulated CP data to quantify the trade-off between the probability of missed detection and the probability of false alarm.

The RADARSAT-2 FQ data acquired over the Strait of Gibraltar are accompanied by simultaneously acquired automatic identification system (AIS) data. The targets detected in quad polarization and simulated CP SAR data were validated using the AIS data.

Quad polarization, dual polarization (including simulated CP and HH + HV with amplitude only), and single polarization (HH) images of known ships were then considered: the relative detection performance of these various SAR systems was estimated by determining the receiver operating characteristics (ROC).

In further work, detection algorithms based on a likelihood ratio test have been optimized and the decision variable derived using the likelihood ratio test has been sent to a K-distribution constant false alarm rate (KCFAR) detector to perform the pixel-based detection. The algorithms for calculating the decision variable from quad polarization data was implemented by the Defence R&D Canada – Ottawa (DRDC Ottawa) using the Analysts' Detection Support System (ADSS), which was developed by the Defence Science and Technology Organization (DSTO, Australia). The KCFAR detector used in this study was developed by the Defence Science and Technology Laboratory (Dstl, U.K.) in ADSS. Initial results demonstrate that KCFAR PolSAR

(KCFAR_Quad) detection algorithms can potentially be effective for detection of small ships ($l \approx 18$ m).

The KCFAR_Quad detection algorithms described in this report provide a performance baseline for PolSAR ship detection.

Results: The results clearly demonstrate that significant improvement in ship detection is possible when using RADARSAT-2 FQ data as compared to dual polarization and single polarization modes. The simulated CP SAR data provide significant detection improvement over single polarization systems, as well as conventional dual polarization with amplitude only. The detection performances of quad polarization, dual polarization and single HH polarization have been estimated. A total of eight ships in one scene were studied, for a probability of false alarm of 10^{-4} ; the quad-pol system achieved seven times lower probability of missed detection than single polarization systems; the CP system achieved four times lower probability of missed detection than single polarization systems. For the CP system, the detection performance for five of the ships was significantly better than that of the dual polarization system with amplitude only. For the other three ships, the performance of the dual polarization system was slightly better. Overall, the detection performance of the CP SAR system was judged to be better than that of the dual polarization system while keeping the same swath width.

The results demonstrate the significant performance benefit of the CP SAR as compared to the single polarization HH system, while providing a wider swath coverage than the quad polarization system.

For the cases studied, the smallest detected ship had a length of 18 m and a speed of 0.59 m/s.

The KCFAR_Quad detector provides good results. Thirty ships verified with AIS data in the ocean region in the Strait of Gibraltar image were detected.

Significance: The PolSAR ship detection algorithms using amplitude and phase information of a target in four channels show a significant improvement in ship detection. A unique feature of the phase information of targets obtained from a PolSAR system has been used to reduce the false alarm rate by discriminating between images of the ships and azimuth ambiguities. The PolSAR system can be used to detect smaller ships than dual polarization or single polarization systems.

The RADARSAT Constellation Mission (RCM) will provide CP as an operational mode, which could be beneficial to ship detection activities. It is recommended that the CP mode be considered for wide area surveillance, in particular, for ship detection.

Sommaire

Ship detection using RADARSAT-2 Fine Quad Mode and simulated compact polarimetry data

Chen Liu; Paris W. Vachon; Ryan A. English; Nicholas Sandirasegaram

DRDC Ottawa TM 2009-285; R & D pour la défense Canada – Ottawa; Février 2010.

Introduction : RADARSAT-2 permet notamment d'utiliser des modes de radar à synthèse d'ouverture polarimétrique (PolSAR). Des données de PolSAR aéroporté ont permis de démontrer que ce système offre un meilleur rendement de détection des navires qu'un système à un seul canal. Dans le présent mémoire technique, on a évalué l'application à des données du mode à polarisation en quadrature fin (FQ) de RADARSAT-2 d'algorithmes de détection de navires par PolSAR qui ont été mis au point au moyen de données aéroportées.

Le SAR à polarimétrie compacte (CP) est une approche de SAR à polarisation double. Une méthode possible de CP est l'utilisation d'une polarisation hybride, ce qui consiste à émettre des ondes en polarisation circulaire et à recevoir deux ondes mutuellement cohérentes avec deux polarisations rectilignes orthogonales. Un SAR CP a une bande au sol plus large qu'un système à polarisation en quadrature de même résolution. Dans le présent rapport, le SAR à polarisation hybride est simulé au moyen des données FQ de RADARSAT-2. Des algorithmes de détection des navires par PolSAR sont ensuite appliqués aux données de SAR CP simulées.

Les données en polarisation double (HH + HV) avec amplitude seulement et en polarisation simple ont été extraites des données FQ de RADARSAT-2.

Le test de rapport de vraisemblance avec critère de Neyman-Pearson, issu de la théorie statistique de la décision, a servi à définir une variable de décision. Le rendement de détection a été caractérisé en calculant la courbe ROC (*Receiver Operating Characteristics*) à partir des données FQ de RADARSAT-2 et des données CP simulées afin de quantifier le compromis entre la probabilité de détection manquée et la probabilité de fausse alarme.

Les données FQ de RADARSAT-2 acquises au-dessus du détroit de Gibraltar sont accompagnées de données du système d'identification automatique (AIS) acquises en même temps. Les détections de cibles réalisées au moyen des données à polarisation en quadrature et des données SAR CP simulées ont été validées à l'aide des données AIS.

L'étude a porté sur des images de navires connus obtenues en mode FQ, en mode polarisation double (y compris en mode CP simulée et en mode à émission en polarisation horizontale et à réception en polarisation verticale (HH + HV) avec amplitude seulement) et en mode polarisation simple (HH). Le rendement de détection relatif des différents systèmes de SAR a été évalué en déterminant la courbe ROC (*Receiver Operating Characteristics*).

Au cours d'études subséquentes, des algorithmes de détection fondés sur le test de rapport de vraisemblances ont été optimisés, et la variable de décision définie au moyen du test de rapport de

vraisemblances a été entrée dans un détecteur à taux de fausses alarmes constant à distribution K (KCFAR) en vue d'effectuer la détection simple par pixels. Les algorithmes de calcul de la variable de décision à partir des données de quadruple polarisation ont été appliqués par R & D pour la défense Canada – Ottawa (RDDC Ottawa) au moyen de l'Analysts' Detection Support System (ADSS), mis au point par la Defence Science and Technology Organization (DSTO, Australie). Le détecteur KCFAR utilisé dans le cadre de la présente étude a été développé par le Defence Science and Technology Laboratory (DSTL, R.-U.) dans l'ADSS. Les premiers résultats montrent que les algorithmes de détection PolSAR KCFAR (KCFAR_Quad) pourraient être efficaces pour la détection de petits navires ($l \approx 18$ m).

Les algorithmes de PolSAR KCFAR décrits dans le présent rapport serviront de référence de rendement pour la détection de navires par PolSAR.

Résultats : Les résultats montrent clairement que l'utilisation de données FQ de RADARSAT-2 permet d'améliorer grandement la détection des navires par rapport aux modes à polarisation double ou simple. Les données de SAR CP offrent une amélioration marquée du rendement de détection par rapport aux systèmes à polarisation simple et aux systèmes à polarisation double classiques avec amplitude seulement. Le rendement de détection des modes à polarisation en quadrature, à polarisation double et à polarisation simple HH a été estimé. La scène étudiée comportait au total 8 navires. Pour un taux de fausse alarme de 10^{-4} , le système à polarisation en quadrature a obtenu une probabilité de détection manquée 7 fois plus basse que le système à polarisation simple, et le système CP a obtenu une probabilité de détection manquée 4 fois plus basse que le système à polarisation simple. Le système CP a obtenu un rendement bien supérieur à celui du système à polarisation double avec amplitude seulement pour 5 des 8 navires. Pour les trois autres navires, le rendement du système à polarisation double était légèrement supérieur. Dans l'ensemble, le système de SAR CP offre un rendement jugé meilleur, tout en gardant la même largeur de bande au sol.

Les résultats démontrent que le SAR CP possède un avantage de rendement marqué sur le système à polarisation simple HH, tout en fournissant une bande au sol plus large que le système à polarisation quadratique.

Pour les cas étudiés, le plus petit navire détecté avait une longueur de 18 m et une vitesse de 0,59 m/s.

L'algorithme KCFAR_Quad donne de bons résultats de détection : dans l'image de la région du détroit de Gibraltar, 33 navires dont la présence dans le secteur a été vérifiée au moyen de données AIS ont été détectés.

Portée : Les algorithmes de détection de navires par PolSAR utilisent l'information d'amplitude et de phase d'une cible provenant de quatre canaux PolSAR afin d'obtenir une amélioration marquée de la détection des navires. Une caractéristique unique de l'information de phase des cibles obtenue d'un système PolSAR a servi à réduire le taux de fausse alarme en éliminant les ambiguïtés sur les navires et les azimuts. Le système PolSAR peut détecter des navires plus petits que les systèmes à polarisation simple ou double.

La mission de la Constellation RADARSAT (MCR) comprendra un mode CP opérationnel, ce qui devrait être avantageux pour le secteur de la détection des navires. Il est recommandé de

considérer la possibilité d'utiliser le mode CP pour la surveillance à grande étendue, en particulier pour la détection des navires.

This page intentionally left blank.

Table of contents

Abstract	i
Résumé	ii
Executive summary	ii
Sommaire	v
Table of contents	ix
List of figures	xi
List of tables	xii
Acknowledgements	xiii
1 Introduction.....	1
2 RADARSAT-2 capabilities	3
3 Overview of methodology	4
3.1 Approach	4
3.2 LRT ship detection	5
3.3 Azimuth ambiguity analysis	6
4 Simulated compact polarimetric SAR	7
5 Data analysis tools	11
5.1 PolSAR tools	11
5.2 IA Pro	11
5.3 ADSS.....	11
6 Data... ..	12
6.1 Polarimetric data.....	12
6.2 AIS data	12
7 Results.....	14
7.1 Quad polarization image.....	14
7.2 LRT ship detection	16
7.3 Phase analysis.....	19
7.4 Compact PolSAR ship detection	27
7.5 Ship detection comparison	28
8 KCFAR ship detection.....	34
8.1 Estimation of K-distribution parameters for quad-pol data.....	34
8.2 Operation of the KCFAR detector.....	35
8.3 Initial detection results	36
9 Conclusions.....	39
References	40
Annex A .. Detection performance	43

List of acronyms	50
------------------------	----

List of figures

Figure 1: RADARSAT-2 operational modes and coverage.	3
Figure 2: Overall detection approach.	4
Figure 3: Graphs of clutter and noise levels for R-2 FQ data.....	9
Figure 4: Physical interpretation of three basic scattering mechanisms.....	14
Figure 5: Pauli-basis RGB image of the Strait of Gibraltar in a geodetic projection.	15
Figure 6: a) Image of ocean decision variable; b) zoom in of an excluded target area from ocean samples in a).	17
Figure 7: Quad-pol detection results of the Strait of Gibraltar in a geodetic projection.	18
Figure 8: Correlation coefficient of HH and VV for test area.....	20
Figure 9: Phase difference between HH and VV for test area.....	21
Figure 10: Correlation coefficient of HV and VH for test area.....	22
Figure 11: Phase difference between HV and VH for test area.....	23
Figure 12: a) Correlation coefficient of HH and VV; b) correlation coefficient of HV and VH; c) phase difference between HV and VH.....	23
Figure 13: Example phase analysis results of HV and VH. a) correlation coefficient for a ship; b) phase difference for a target and an ambiguity; c) phase difference for an ambiguity.....	24
Figure 14: a) $ HV - VH $; b) $ HV $ image of the Strait of Gibraltar.	26
Figure 15: Detection results for simulated CL data of the Strait of Gibraltar in a geodetic projection.....	28
Figure 16: a) Detection performance for ship 3; b) $ HH $ image and c) simulated $ X_1 $ image.	29
Figure 17: a) Detection performance for ship 6; b) $ HH $ image and c) simulated $ X_1 $ image.	30
Figure 18: Probability density function of the ocean decision variable.	35
Figure 19: KCFAR detection results of the Strait of Gibraltar in a geodetic projection.	37
Figure 20: KCFAR detection results. a) and b) land ambiguities; c) a target and its ambiguity..	38
Figure 21: a) Detection performance for ship 1; b) $ HH $ image and c) simulated $ X_1 $ image.	44
Figure 22: a) Detection performance for ship 4; b) $ HH $ image and c) simulated $ X_1 $ image.	45
Figure 23: a) Detection performance for ship 7; b) $ HH $ image and c) simulated $ X_1 $ image.	46
Figure 24: a) Detection performance for ship 8; b) $ HH $ image and c) simulated $ X_1 $ image.	47
Figure 25: a) Detection performance for ship 9; b) $ HH $ image and c) simulated $ X_1 $ image.	48
Figure 26: a) Detection performance for ship 10; b) $ HH $ image and c) simulated $ X_1 $ image. ...	49

List of tables

Table 1: Polarization information hierarchy.....	7
Table 2: Extracted ship information from AIS data (July 29, 2008).	13
Table 3: Absolute correlation coefficients for ocean.....	19
Table 4: Values of P_{MD} for $P_{FA} = 10^{-4}$ for ships considered.....	32
Table 5: Statistical analysis results of detection performance for $P_{FA} = 10^{-4}$	33

Acknowledgements

The authors would like to thank Mr. John Wolfe (DRDC Ottawa) for obtaining the MSSIS data and for helpful discussions and Mr. Tom Lukowski (DRDC Ottawa) for his constructive comments to improve the report.

The authors would like to thank the participants in the compact polarimetry working group that is led by the Canada Centre for Remote Sensing (CCRS), particularly, Dr. Brian Brisco for his leadership and Dr. François Charbonneau for his technical insight.

The authors would also like to thank Mr. Adam Klein (MDA) for his implementation of the quad polarization ship detection algorithms in ADSS, that were based on the likelihood ratio test, the decision variable and the KCFAR detector.

This page intentionally left blank.

1 Introduction

RADARSAT-2, a Canadian satellite, has been successfully operating in space since late 2007. It carries a synthetic aperture radar (SAR) that provides many operating modes, including the Fine Quad (FQ) Mode, which provides polarimetric phase and amplitude information.

Improvements in ship detection capabilities by use of a polarimetric SAR (PolSAR) system have previously been demonstrated using airborne PolSAR data [1]. This report shows that RADARSAT-2 FQ imagery also provides an improvement in detection performance. It was shown in [1] that quad polarization gives the best performance, followed by dual polarization systems, which in turn are better than single polarization systems.

One objective of this report is to describe the use of FQ data to evaluate the performance of several types of SAR systems: single polarization HH, dual polarization, horizontal polarization on transmit and horizontal and vertical polarizations on receive (HH + HV) amplitude only, quad polarization, and compact polarimetric (CP). The decision variable used for the detectors is based on the likelihood ratio test with the Neyman-Pearson criterion as defined in [1]. The detection performance is estimated on the basis of the receiver operating characteristic (ROC) [2].

CP radar is a two channel approach to polarimetric synthetic aperture radar [4]. It can provide a wider swath than quad polarization because it uses two channels rather than four. For maritime surveillance applications, wide swath coverage is essential to maximize the area coverage. For example, RADARSAT ScanSAR Narrow B (SCNB) Mode images acquired using dual polarization are very favourable for ship detection [5] because of the wide swath width. There are several CP configurations including the $\pi/4$ mode and two alternative compact modes. In the $\pi/4$ mode, a linearly polarized wave at a 45° orientation is transmitted and linear H and V polarized waves are received [6][7]. In the alternative compact modes, a circularly polarized wave is transmit and like and opposite circularly (Compact Circular – C,C), or linearly H and V polarized waves (Compact Linear – CL) are received. The CL mode is also referred to as hybrid-polarity [4][7].

In this study, right-circular transmit and linear receive (i.e., hybrid-polarity, CL) data were simulated using RADARSAT-2 FQ data. The application of PolSAR ship detection algorithms developed using airborne data to the simulated CL data was investigated.

SAR data of the Strait of Gibraltar, which contain many target ships, acquired using RADARSAT-2 FQ, were used, along with simultaneously acquired shore-based automatic identification system (AIS) data. Detected targets were validated using the AIS data.

The second objective is to optimize the detection algorithms based on the likelihood ratio test. This study demonstrates that the probability density function (PDF) of the ocean decision variable follows approximately a K-distribution. Thus, the algorithms based on the likelihood ratio test have been merged with a K-distribution constant false alarm rate (KCFAR) detector. Taking an advantage of existing KCFAR detector in the Analysts' Detection Support System (ADSS), which was developed by the Defence Science and Technology Organization (DSTO, Australia) [3], the merged algorithms have been implemented by the Defence R&D Canada (DRDC).

In this report, Section 2 provides a summary of RADARSAT-2's capabilities; Section 3 presents the methodologies used in this study; Section 4 describes CP SAR; Section 5 contains a discussion of the data analysis tools; Section 6 summarizes the data used in this study; Section 7 presents the results; Section 8 describes the KCFAR_Quad detector using the ADSS and the initial detection results; and Section 9 presents the conclusions.

2 RADARSAT-2 capabilities

RADARSAT-2 is a C-band (5.405 GHz) SAR satellite. The system includes polarimetric SAR capability and supports right- and left-look imaging. A number of imaging modes provide a trade-off between spatial resolution and swath coverage. The high-resolution, narrow-swath width modes, such as Ultrafine, have a nominal resolution of 3 m with a swath coverage of 20 km. In contrast, the low-resolution, wide-swath width modes, such as ScanSAR Wide, have a nominal resolution of 100 m with a swath coverage of 500 km. Certain modes are available in a choice of single, dual or quad polarization. The operational modes and the coverage are illustrated in Figure 1 [8]. RADARSAT-2 was launched in December 2007; it is owned and operated by MacDonald Dettwiler and Associates Ltd [9].

In this report, we focus on the FQ Mode. In FQ, the SAR transmits horizontal and vertical polarized electromagnetic waves on alternate pulses and receives the scattered signal in both polarizations simultaneously. The quad polarization data consist of amplitude and phase information of measured scattered fields from a target. The additional phase information aids in target classification.

The FQ Mode is intended for applications that require polarimetric information (i.e. amplitude and phase) of a target, but this is done with a trade-off of narrow swath coverage. The FQ Mode can cover an incidence angle range from 20° to 41° with many beam positions; each beam position “covers” approximately 2° . Only one beam position can be used during each image acquisition. The incidence angle is defined as the angle between the line of sight from the radar and the local vertical direction. The nominal resolution is $5.4 \text{ m} \times 7.9 \text{ m}$ (slant range \times azimuth) for single look complex (SLC) data and the scene size is approximately $25 \text{ km} \times 25 \text{ km}$.

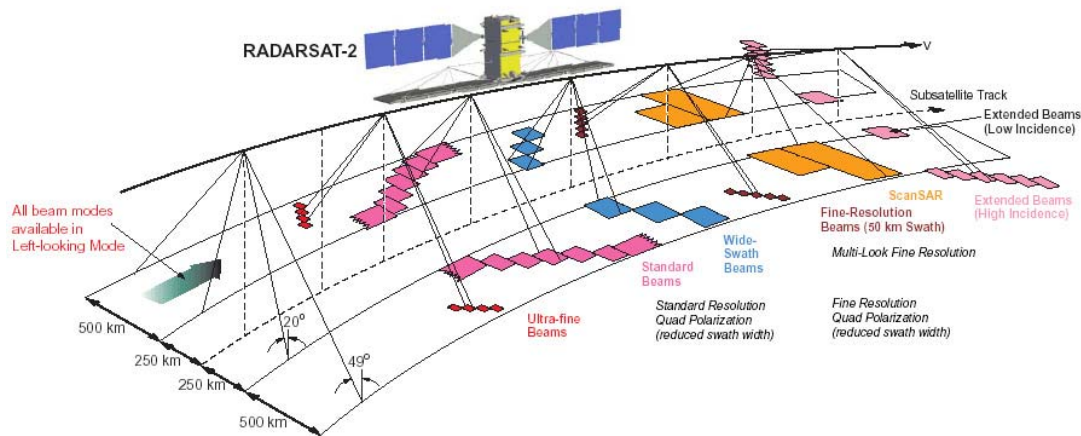


*Figure 1: RADARSAT-2 operational modes and coverage.
(used with permission [8])*

3 Overview of methodology

3.1 Approach

The overall approach to PolSAR ship detection in this study consists of many steps as illustrated in Figure 2. The most important step is the ship detection. This is followed by verification using AIS data. If a detected candidate target has corresponding AIS data, then the candidate target is confirmed as a ship. If the candidate target does not have AIS data, ambiguity discrimination using phase analysis is used. In this report, we focus on algorithms developed at DRDC, including target detection and azimuth ambiguity analysis.

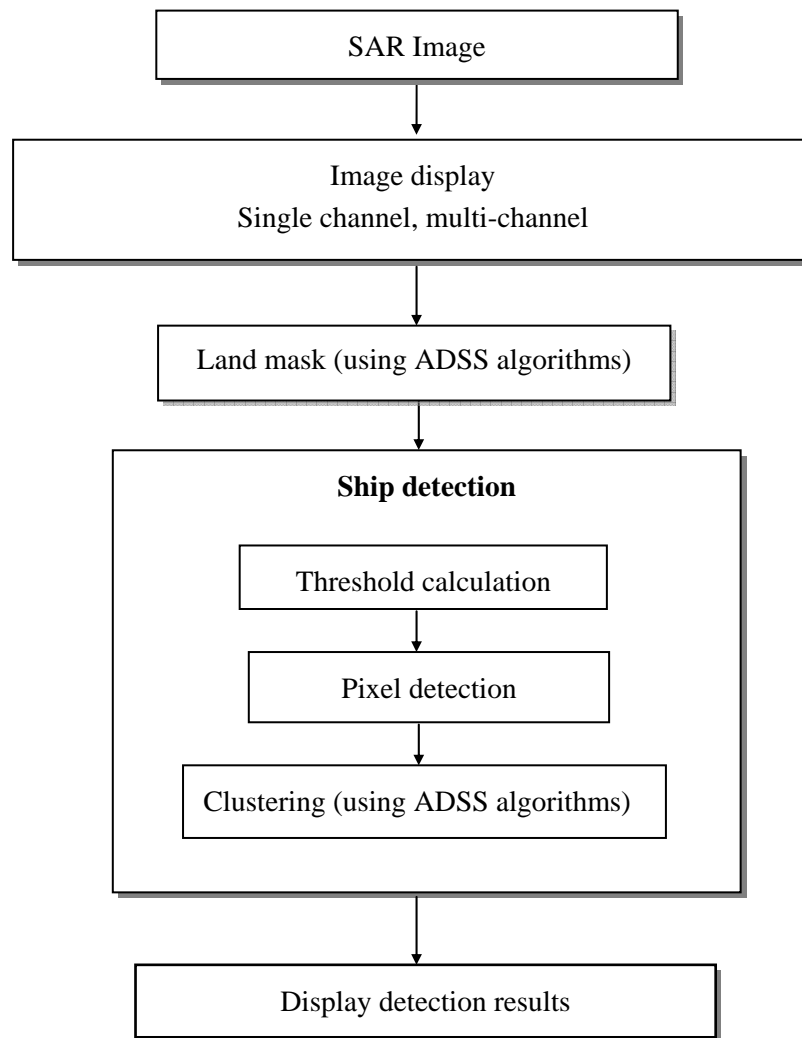


Figure 2: Overall detection approach.

3.2 LRT ship detection

The methodology of likelihood ratio test (LRT) ship detection using polarimetric SAR data has been described in [1]. A polarimetric SAR system provides observations of the scattering matrix $\mathbf{X}(i, j)$ for each pixel (i, j) in an image. The matrix components $S_{HH}(i, j)$, $S_{HV}(i, j)$, $S_{VH}(i, j)$ and $S_{VV}(i, j)$ give the transformation between the transmitted and scattered electromagnetic fields. These consist of the amplitude and phase of each of the four channels of the polarimetric data. The components of $\mathbf{X}(i, j)$ can be written as a vector:

$$\mathbf{X}(i, j) = [S_{HH}(i, j) \ S_{HV}(i, j) \ S_{VH}(i, j) \ S_{VV}(i, j)]^T \quad (1)$$

where the superscript T is the transpose operator.

Ship detection is a binary decision problem. In the fundamental algorithms of polarimetric SAR ship detection, statistical decision theory is applied directly to the components of the scattering matrix to obtain a decision variable. A likelihood ratio test with the Neyman-Pearson criterion is used to define a pixel-based detection criterion. Gaussian distributions for each of the scattering matrix components are assumed to derive the formulation while measured data are used to calculate the detection variables.

The decision variable is approximately given by [1]:

$$\mathbf{X}^H (C_o^{-1}) \mathbf{X} = \begin{cases} > \eta & \text{for a ship} \\ \leq \eta & \text{for ocean} \end{cases} \quad (2)$$

where $C_o = E(\mathbf{X}\mathbf{X}^H)$ is the covariance matrix of the ocean, $E(\cdot)$ is the expectation operation, H is the Hermitian transpose operator and η is the designed detection threshold.

As shown in [1], this methodology can be applied to dual polarization and single polarization systems. In a dual polarization system, the vector $\mathbf{X}(i, j)$ has two elements and in a single polarization system, $\mathbf{X}(i, j)$ has one element.

A detection threshold is calculated based on a specified false alarm rate (FAR) which is interpreted as the probability of false alarm (P_{FA}) by using a combination of extrapolation and curve fitting methods [11].

As shown in [1], a statistical decision variable is calculated for each pixel of the selected ocean areas in the image using Equation (2). This is followed by the calculation of the median value. The median is used as an initial threshold value because it is less affected than the mean by the presence of large pixel amplitudes if ships are present. Finally, the other thresholds are calculated in increments of half of the median. A curve of P_{FA} as a function of these thresholds is then determined. The number of pixels is limited in the selected ocean area, consequently, the P_{FA} obtained from the measured data is limited. In order to obtain a specified P_{FA} , such as 10^{-6} or 10^{-8} , an extrapolation method is used. A 2nd order polynomial is fitted to the data points (P_{FA} versus threshold) using a minimum mean square error method. The 2nd order polynomial equation is then used to calculate the threshold for the desired P_{FA} [11].

Estimation of detection performance is provided by ROC curves, which are a plot of the probability of missed detection (P_{MD}) versus probability of false alarm (P_{FA}). These probabilities are determined by varying the detection threshold.

The algorithms described here are for pixel-based detection; complete ship detection is performed after pixel detection by using a clustering technique. (Examples can be found in [3].) The P_{FA} specified in this report is for pixel detection. The application of clustering will reduce the overall P_{FA} for ship detection because more than one detected pixel is required to declare the presence of a target.

3.3 Azimuth ambiguity analysis

In a radar image, azimuth ambiguities arise due to discrete sampling of the Doppler spectrum at the interval of the pulse repetition frequency (PRF or f_p) [12]. Since the Doppler spectrum repeats at f_p intervals, the sampled signal components outside of this frequency interval will be aliased into the central region of the spectrum. Ambiguities are often detected as candidate targets in the maritime environment since the clutter (ocean) signal may be low. However, azimuth ambiguities can be distinguished from the main target image by using analysis of the phase.

Under the reciprocity assumption, the HV and VH channels are identical (i.e., $S_{HV} = S_{VH}$ for both amplitude and phase). Also, the phase difference between samples in the HV and VH channels is zero for targets and even-order azimuth ambiguities, but is π for odd-order azimuth ambiguities [13]. This phase difference between the HV and VH channels can be used to discriminate between targets and odd-order azimuth ambiguities.

The azimuth shift of the ambiguity location relative to the true target location can be determined [14]:

$$\Delta X_{amb} = \frac{\lambda R f_p}{2V_s} \left(1 - \frac{\omega_e}{\omega} \cos(\varphi) \right)^{-1} \quad (3)$$


where λ is the radar wavelength, R is the slant range at which the target is broadside to the radar, V_s is the spacecraft velocity, ω_e is the earth rotation speed ($2\pi/\text{day}$), ω is the spacecraft orbital rate (343 orbits in 24 days) and φ is the inclination of the orbit of the spacecraft.

4 Simulated compact polarimetric SAR

CP is a type of dual channel synthetic aperture radar in which one polarization is transmitted, but two orthogonal polarizations are received, providing both phase and amplitude information of the measured backscattered fields. Target backscatter information is available through access to Stokes parameters. However, a CP system cannot provide “pure” HH or VV backscatter information and cannot be considered to be a substitute for a quad-pol system.

A quad-pol system is expected to provide the best ship detection results compared to other SAR systems at the same resolution [1] since it contains full characterization of the backscattered field, but at the expense of a narrow swath. A CP system is expected to benefit ship detection when compared to single-polarization and conventional dual-polarization systems since it contains relative phase information between the two receive channels. The CP system requires only one-half of the data volume per pixel compared to a quad-pol system, so it should be possible to achieve a wider swath width than a quad-pol system (i.e., double the swath width). The trade-off between the information, swath width and system complexity for the same resolution is clearly demonstrated in the polarization information hierarchy table (Table 1).

Table 1: Polarization information hierarchy.



Mode	Transmit	Observe	Swath
SINGLE POLARIZATION	H or V	S_{HH} or S_{VH} or S_{HV} or S_{VV}	Wide
ALTERNATING POLARIZATION	H and V	(S_{HH}, S_{VV}) (no phase)	Wide
DUAL POLARIZATION ON RECEIVE	H or V	(S_{HH}, S_{HV}) or (S_{VV}, S_{VH})	Wide
COMPACT POLARIMETRY (CL MODE)	Circular	$(S_{HH} - jS_{HV})/2^{1/2}$ $(S_{VH} - jS_{VV})/2^{1/2}$	Wide
QUAD POLARIZATION	H and V	$S_{HH}, S_{HV}, S_{VH}, \& S_{VV}$	Narrow

The various possible CP modes have been presented in Section 1. Comparison of these CP SAR modes has been discussed in the literature e.g. [4][7][15]. For example, it has been shown that the well-known Cloude-Pottier entropy-alpha classification can be performed using the CL system and the $\pi/4$ mode is

almost as good as full quad-pol for crop classification [15]. Also, circular polarization on transmission is preferred when there is Faraday rotation in the propagation medium [7]. In addition, the architecture of a CL system is relatively simple [4].

In the context of this study, the received components of a CL system consist mostly of S_{HH} and S_{VV} because cross-pol components are usually small. It has been shown that a dual-pol system that uses HH and VV polarization combinations provides good ship detection performance [1]. It has also been shown that the detection performance of HH and VV is usually better than for conventional dual-pol systems with single transmit polarization (HH and HV, or VV and VH). Therefore, it is expected that a CL system should also be capable of better ship detection performance than conventional dual-pol systems and this is possible with a wider swath than a quad-pol system.

Right-circular transmit and linear receive SAR can be simulated from RADARSAT-2 FQ data as shown in [4] and [16]:

$$\mathbf{X} = S \circ \mathbf{J} = \begin{bmatrix} S_{HH} & S_{HV} \\ S_{HV} & S_{VV} \end{bmatrix} \circ \frac{1}{\sqrt{2}} \begin{bmatrix} 1 \\ -j \end{bmatrix} = \frac{1}{\sqrt{2}} \begin{bmatrix} S_{HH} - jS_{HV} \\ S_{VH} - jS_{VV} \end{bmatrix} \quad (4)$$

where \mathbf{J} is the Jones vector. The scattering matrix components are taken from the measured RADARSAT-2 FQ data.

If we also consider system noise effects, then the terms of the \mathbf{X} vector for the CL system become:

$$\mathbf{X} = \frac{1}{\sqrt{2}} \begin{bmatrix} (S_{HH} + N_1) - j(S_{HV} + N_2) \\ (S_{VH} + N_3) - j(S_{VV} + N_4) \end{bmatrix} \quad (5)$$

where N_1, N_2, N_3 and N_4 are the receiver noise in each channel [16]. The signal and noise components in each channel are assumed to be Gaussian and independent, with identical noise power $E(|N|^2)$. Using the independence properties of the signal and noise components, it can be shown that the system power in each channel is:

$$E(|X_1|^2) = \frac{1}{2} E(|S_{HH}|^2 + jS_{HH} \cdot S_{HV}^* - jS_{HV} \cdot S_{HH}^* + |S_{HV}|^2 + 2 \cdot |N|^2) \quad (6)$$

$$E(|X_2|^2) = \frac{1}{2} E(|S_{VH}|^2 + jS_{VH} \cdot S_{VV}^* - jS_{VV} \cdot S_{VH}^* + |S_{VV}|^2 + 2 \cdot |N|^2) \quad (7)$$

where E is the expectation operator. An actual CP system would have half the noise power in each channel compared to a CP system simulated using RADARSAT-2 FQ data. However, the main terms contributing in each channel are co-pol terms, i.e., S_{HH} and S_{VV} , which are usually strong signals.

The system performance is approximately determined by the effective target to clutter ratio of the signal components. The effect of the noise is to increase the apparent power of each signal component.

Typical system noise data for the image which was used is illustrated in Figure 3, which shows the levels of co-pol and cross-pol clutter relative to the system noise floor. The noise, taken from the product meta data, is expressed as noise equivalent sigma zero (NESZ). The NESZ graph of Figure 3 represents the noise in the HH channel whose power is approximately the same as that in other channels. In the top graph, the backscatter (σ^0 , or σ^0) of each channel (HH, HV, VH, and VV) is shown for the area of interest, while in the bottom graph, the σ^0 is shown across the entire range for the same azimuth area as the top graph.

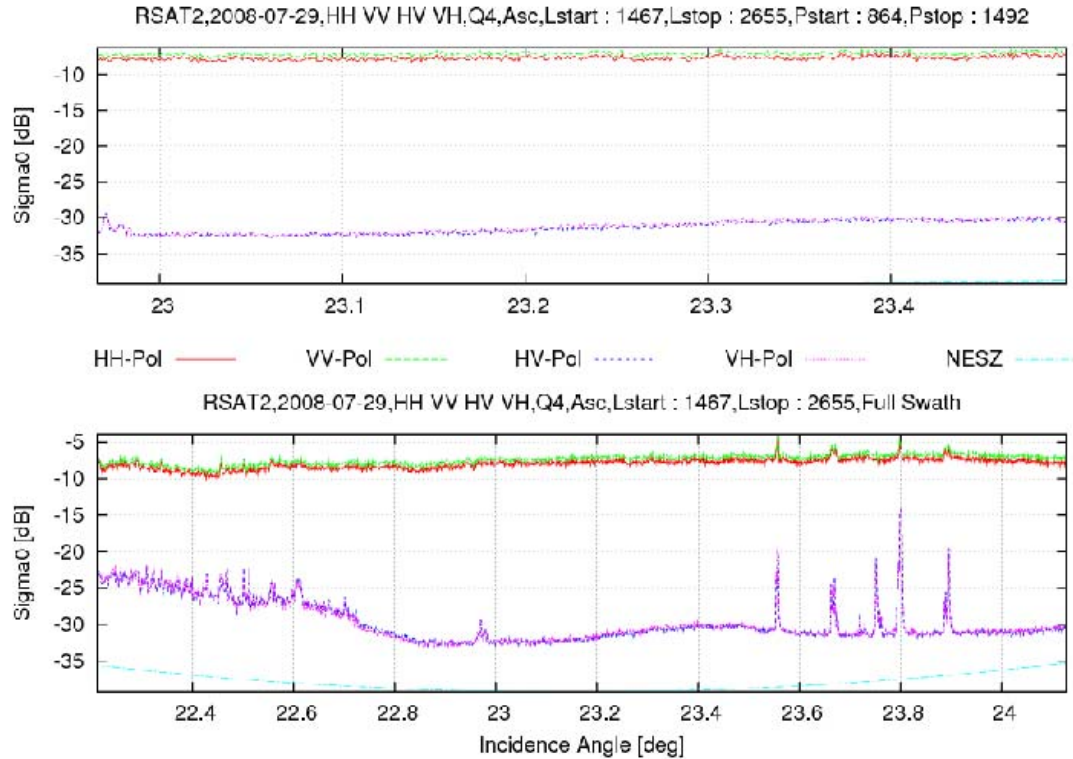


Figure 3: Graphs of clutter and noise levels for R-2 FQ data.

In the case of Figure 3, the clutter to noise ratio for the co-pol components of the ocean clutter is about 30 dB, while the clutter for the cross-pol components is only about 6 dB above the noise floor. The noise power in each channel of the simulated CL product is increased by 3 dB compared to single channel because noise from both co-pol and cross-pol channels is present. The clutter to noise ratio at each linear polarization component will thus be decreased by 3 dB.

Figure 3 also shows a number of targets in the cross-pol transect that have target to clutter ratios ranging from 7 to 16 dB. The cross-pol targets, which are 13 to 22 dB above the noise, will have their

apparent levels raised by 0.2 to 0.03 dB respectively. The co-pol clutter apparent level will be increased by only about 0.004 dB compared to the level without noise because it is 30 dB above the noise. Thus, the target to clutter ratio for the cross-pol components will be lowered by less than 1 dB compared to the value without noise while the target to clutter ratio of the co-pol components will be degraded by a negligible amount.

For the simulated CL system, Equations (6) and (7) show that each channel will contain a co-pol component as well as cross-pol components and a doubled noise power. The dominant component of each channel is the co-pol component. The co-pol clutter-to-noise ratio will now be about 27 dB because of the doubled noise and the apparent level of the co-pol component will be increased by about 0.009 dB, which is still negligible. The levels of target signals will also be unaffected by the noise because they are much larger than the clutter. Thus, the effective target-to-clutter ratio of each channel of the simulated CL system will be negligibly affected by the presence of the noise.

It is concluded that using R-2 FQ Mode data to simulate the CL system will provide a realistic performance estimate which is unaffected by the system noise because the received signal channels are dominant by the co-pol components.

5 Data analysis tools

5.1 PolSAR tools

Most of the data analysis tools used in this study were developed at DRDC Ottawa. These tools include the Likelihood Ratio Test PolSAR Ship Detector, polarization synthesis, phase analysis and target signature analysis, as described in Section 3 and Figure 2. The tools were developed in Matlab™.

5.2 IA Pro

In this report, some of the results are displayed using Image Analyst Pro (IA Pro) which was developed at DRDC Ottawa for validation and demonstration of new algorithms for GEOINT [17]. The focus of IA Pro development is on tools that introduce automation, feature extraction and image combination/fusion to the exploitation of SAR and EO imagery. IA Pro provides support for single- and multi-channel SAR and EO imagery, and permits the image analyst to incorporate geospatial information (i.e., thematic vector layers and digital maps) for contextual awareness.

IA Pro was built using C++, Python, OpenEV and the Geospatial Data Abstraction Library (GDAL). Python is an open-source object-oriented interpreted programming language, OpenEV is an open-source library of raster and vector classes and functions, and GDAL is a translator library for raster geospatial data formats. IA Pro provides a multitude of tools for the manipulation and exploitation of multi-sensor and multi-temporal imagery for GEOINT. A detailed description of IA Pro can be found in [17].

5.3 ADSS

The Analysts' Detection Support System is an extensible suite of image processing algorithms for GEOINT applications – including automatic target detection (ATD) for broad-area search for small targets – with SAR and EO/IR sensors [3]. It was developed by DSTO, with additional contributions from the Defence Science and Technology Laboratory (Dstl) and DRDC. ADSS includes algorithms for ATD, change detection, and region classification for both maritime and land areas, in addition to a number of support and utility modules. The flexibility of ADSS arises from a system architecture that supports the combination of algorithms in a user-specified structure. (The numerous algorithms and utilities that are provided by ADSS are implemented as modules that can be combined by using Command and Data Language (CDL) scripts.) The power of ADSS originates in a framework that provides for synchronization, control, and data flow between the various modules.

In the second part of this study, a popular and widely used ATD algorithm the K-distributed constant false alarm rate (K-CFAR) algorithm (KCFAR module) implemented in ADSS [18] [19] was applied to the data. The KCFAR module uses the K-distribution to model the probability density function (PDF) of inhomogeneous ocean clutter and system noise in high-resolution SAR images. The KCFAR module locally estimates the parameters for the K-distribution and assigns detections to bright points appearing in the tail of the distribution.

6 Data

6.1 Polarimetric data

The polarimetric data used in this study were acquired in RADARSAT-2 FQ Mode on 29 July 2008 (PDS_00278000). The Strait of Gibraltar was chosen since there are many ships in this region and there are validation data available from AIS. The data were acquired on an ascending pass and the nominal incidence angle range is from 22° to 24°. The signal data were processed to a calibrated image by MDA. Radar backscatter coefficient (σ^0) values were used in this analysis.

6.2 AIS data

AIS is an internationally mandated ship-based transponder system [19] that is used by vessels to inform one another about their activity. Information available includes identity, location, speed, heading, type, International Maritime Organization (IMO) number, and Maritime Mobile Service Identity (MMSI) number. This system is designed primarily for safety of life at sea (SOLAS), collision avoidance and traffic management. AIS operates in the VHF maritime band using a Self-Organized Time Domain Multiplex (SOTDMA) protocol that coordinates communication between vessels within line-of-sight; shore-based, air-based, or space-based receivers can also receive this information. Although this cooperative identification system is intended for collision avoidance, it is available to assist maritime wide area surveillance by providing vessel identities.

AIS data were acquired along with the RADARSAT-2 data and are used to verify identities and locations of ships detected in this study. The AIS data were obtained from the Maritime Safety and Security Information System (MSSIS) which was initiated by the US Coast Guard. International contributors gain access to the database which is generated from real time reports from shore-based receivers. The MSSIS data used for this report were provided by DRDC Atlantic and processed at DRDC Ottawa [5].

Ten ships for which AIS data are available have been used in this and other separate studies. Eight of them have been selected for detection performance analysis (Section 7.5). Ship information, such as length, width, speed and type can be extracted from the AIS data, as listed in Table 2.

Table 2: Extracted ship information from AIS data (July 29, 2008).

Ship	Speed (knots)	Width (m)	Length (m)	Draught (m)	Type
1	0	30	258	7.8	Cargo
2	1.1	42	332	11.8	Tanker
3	0.3	32	181	10.1	Tanker
4	0.3	49	288	10.5	Tanker
5	1.1	6	18	4.2	Tug
6	16.1	30	198	10.6	Cargo
7	0.7	44	277	10.2	Tanker
8	15.2	60	333	11.5	Tanker
9	10.35	25	184	7	Cargo
10	0.22	26	198	8	Tanker

7 Results

7.1 Quad polarization image

A quad polarization image can be displayed in many ways, for example as a single channel in grey scale or a linear combination of four channels in an RGB color image. In this study, the Pauli-basis RGB display is used since it permits the extraction of physical information. In a Pauli-basis image, the $S_{HH} + S_{VV}$ component represents single (odd) bounce scattering, while $S_{HH} - S_{VV}$ represents double (even) bounce, and $S_{HV} + S_{VH}$ represents volume scattering. The physical interpretation of these three basic scattering mechanisms is illustrated in Figure 4.

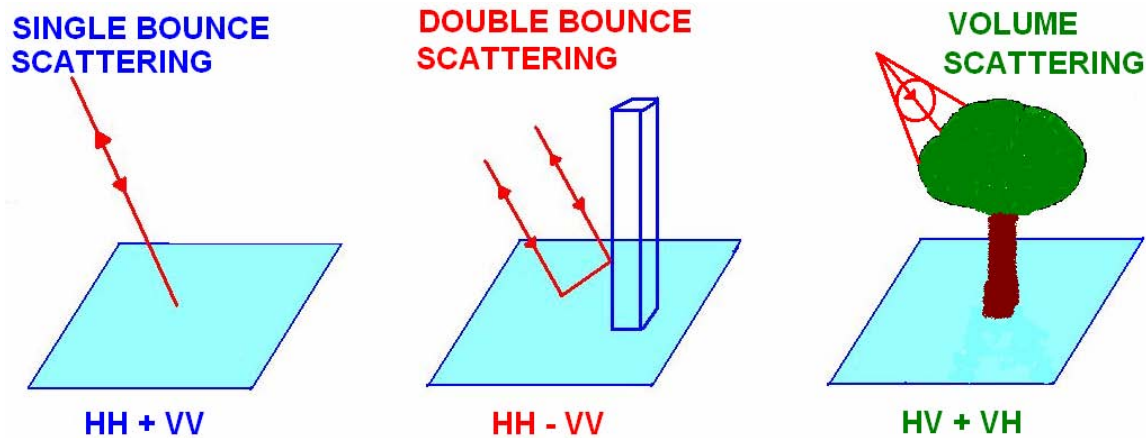


Figure 4: Physical interpretation of three basic scattering mechanisms.

The Strait of Gibraltar image which is used as a test image is displayed in the Pauli-basis in Figure 5. In this image, the magnitude of $a \times |HH - VV|$ is displayed in red, the magnitude of $b \times |HV + VH|$ is displayed in green, and the magnitude of $c \times |HH + VV|$ is displayed in blue. The coefficients a , b , and c are selected to be 2, 3 and 1 respectively. The ocean tends to exhibit single bounce scattering, while ships tend to have a significant amount of double bounce scattering. Vegetation tends to have significant volume scattering in addition to surface scattering.

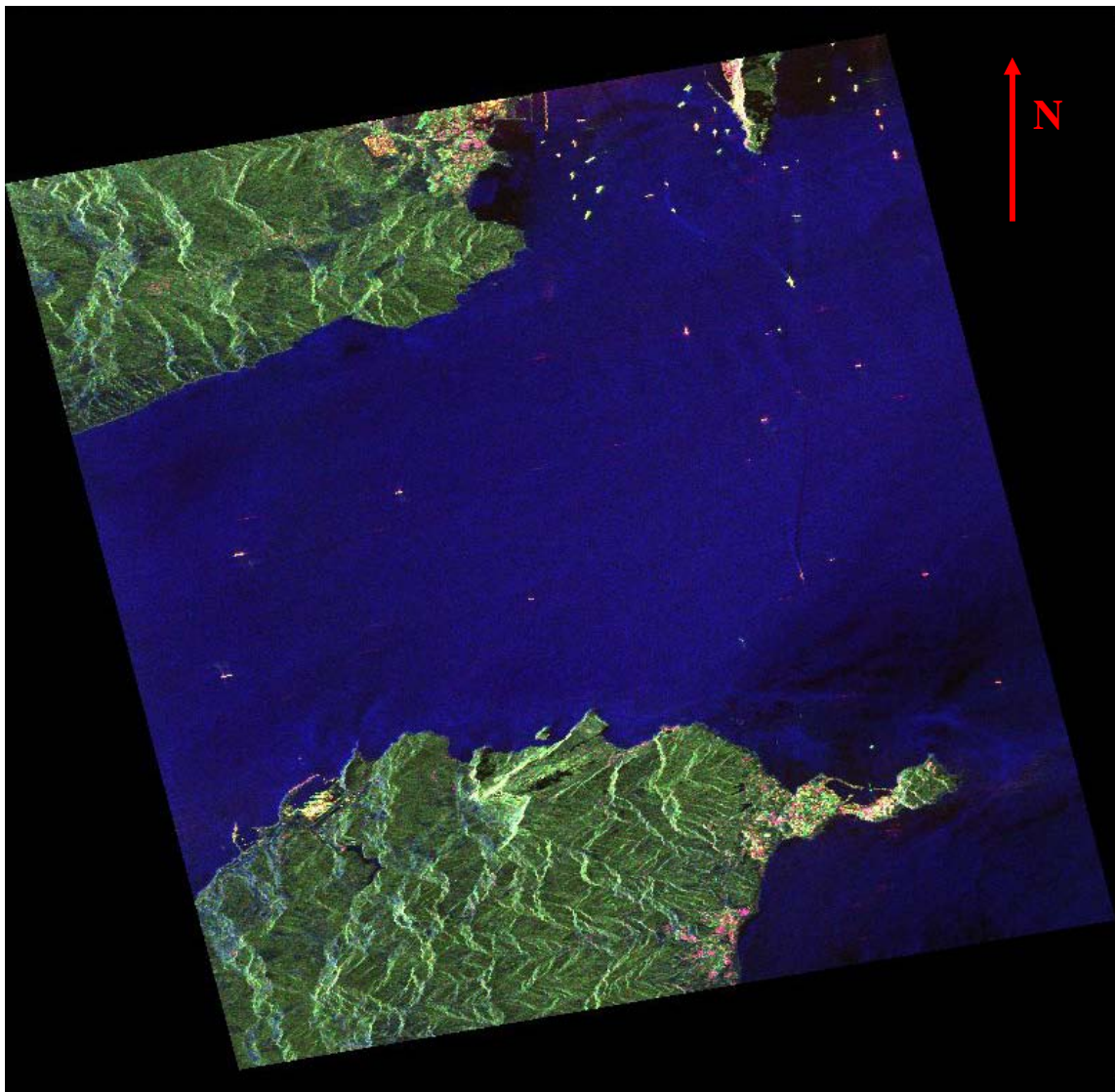


Figure 5: Pauli-basis RGB image of the Strait of Gibraltar in a geodetic projection.

Original RADARSAT-2 Data and Products ©MacDonald, Dettwiler and Associates Ltd., 2008 – All Rights Reserved.

7.2 LRT ship detection

The Likelihood Ratio Test (LRT) Ship Detection software was applied to the test image and the detection threshold was calculated based on a specified probability of false alarm (P_{FA}) using a combination of the extrapolation and curve fitting methods, as described in Section 3 and in [11].

In order to calculate the threshold, we need to select an area of the ocean. In this example, the ocean area (range pixels: 1000 to 1300 and azimuth pixels: 1600 to 2600) consists of approximately 3×10^6 pixels. The detection threshold is approximately 16 dB and is calculated with the P_{FA} set to 10^{-6} for detection in the quad-pol image. The images of the ocean decision variable used to calculate the threshold are illustrated in Figure 6a) and b). In Figure 6a), we can see that there is a candidate target in the selected ocean region.

In order to reduce or even eliminate the effect of pixels with high decision variable values (i.e. potential targets or land) on the calculation of the threshold, two steps were involved in the calculation. The detection variable is estimated from the selected ocean. Then, the threshold was calculated using only pixels which have decision variable values less than 3 times the median of the decision variable, as illustrated in Figure 6b), which indicates that candidate target was excluded (appears black in the image since the values are zero). Figure 6b) is a zoom in of the target location in Figure 6a).

In this section, the focus is on the application of the detection algorithms. Optimization of the detection is described later in this document.

The detection results are shown in Figure 7 where pixels having values smaller than the detection threshold were assigned to be zero and the pixel values were retained for pixels having values greater than the threshold. In Figure 7, the green boxes indicate locations where ship signatures are predicted to be based on the MSSIS AIS data and the image acquisition parameters. Based on the available AIS data, 34 out of 36 ships were detected and the smallest of these had a length of 18 m and a speed of 0.59 m/s. Two ships identified in the AIS data were not detected by the PolSAR detector. One of them was very close to land, as indicated in this figure.

An example of a detected unknown ship target is indicated as T_u . The azimuth ambiguity of this target was also detected as a candidate target (A_u). It has been found that azimuth ambiguities can be distinguished from targets because of their phase characteristics, as discussed in the next section.

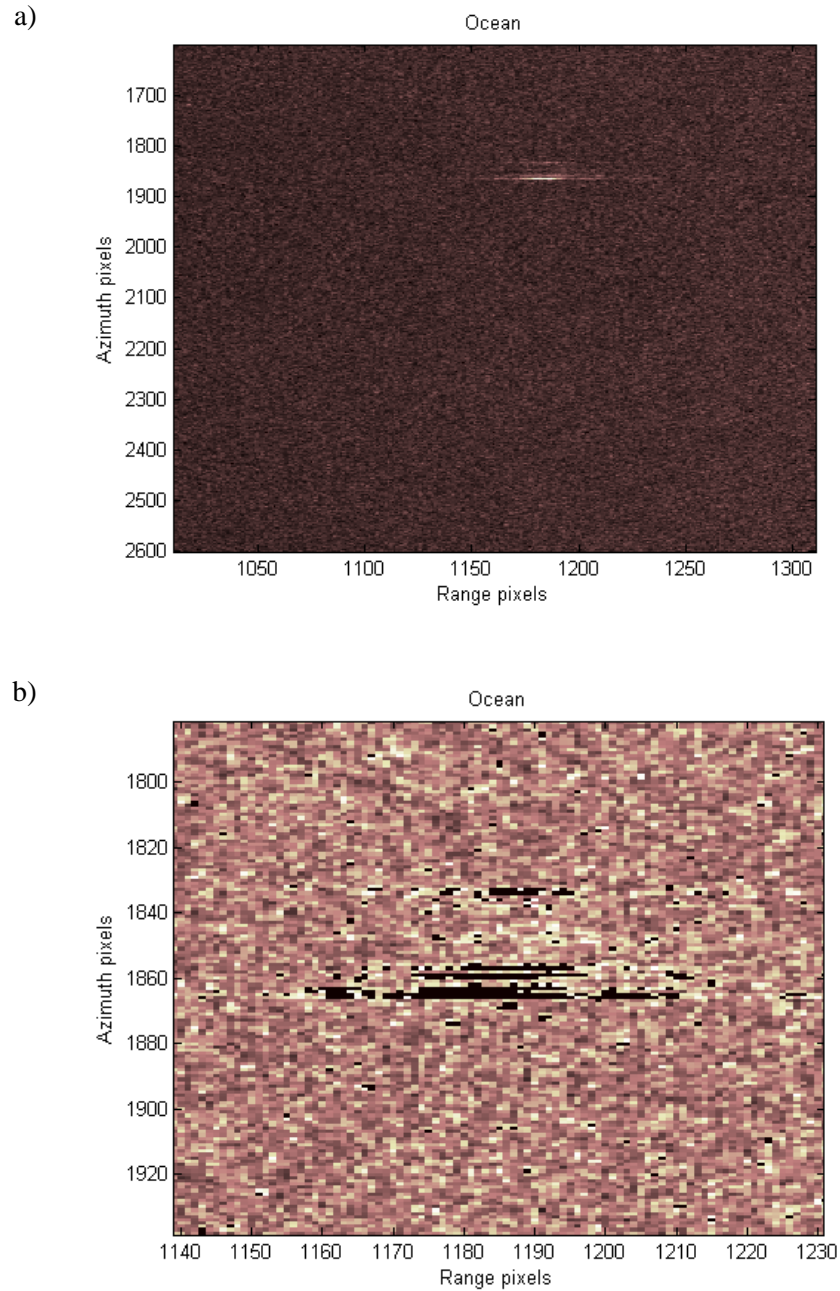
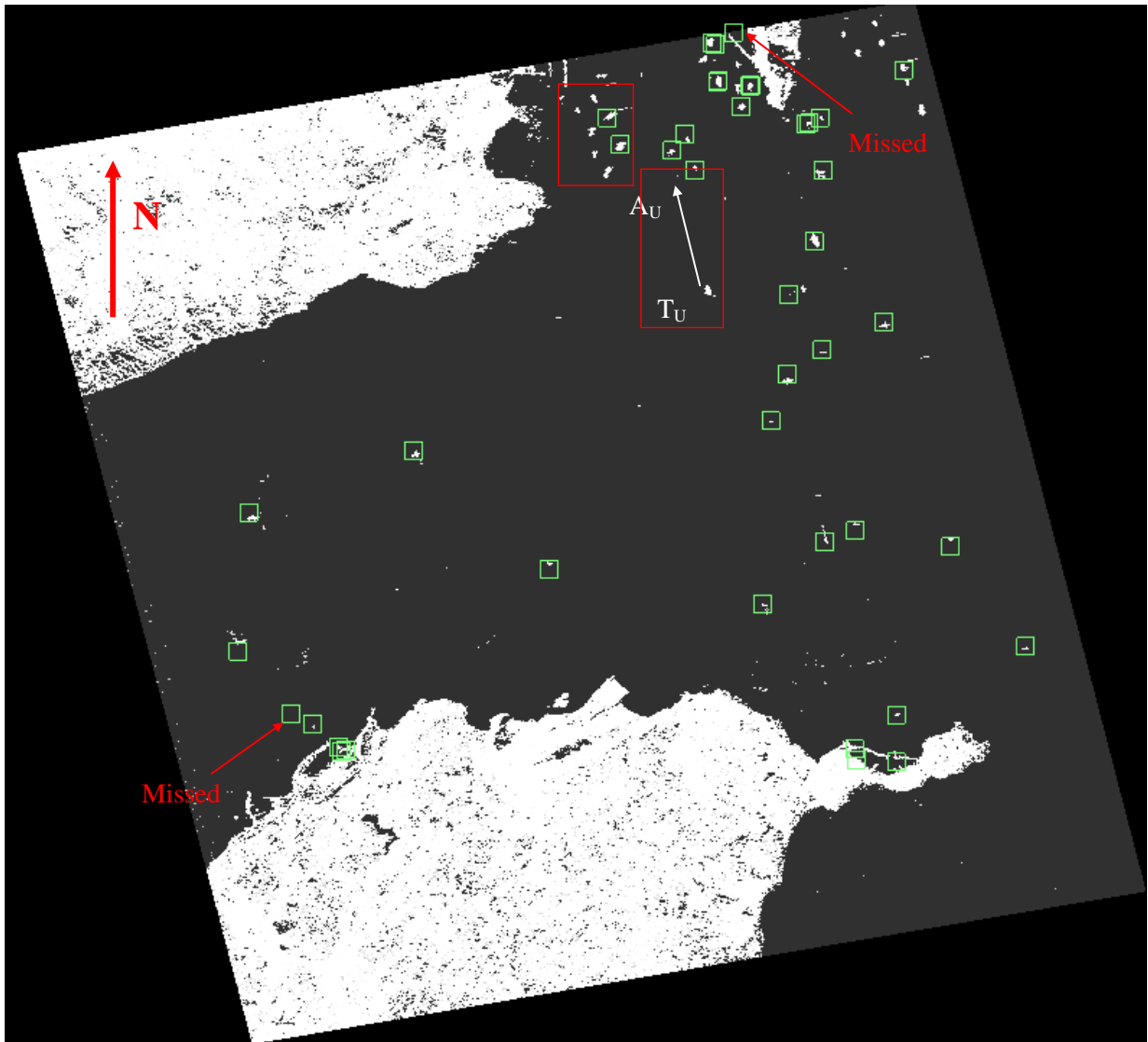


Figure 6: a) Image of ocean decision variable; b) zoom in of an excluded target area from ocean samples in a).

Original RADARSAT-2 Data and Products ©MacDonald, Dettwiler and Associates Ltd., 2008 – All Rights Reserved.



AIS
 Target of interest (see Figure 12 and 13)

Figure 7: Quad-pol detection results of the Strait of Gibraltar in a geodetic projection.

Original RADARSAT-2 data and products © MacDONALD, DETTWILER AND ASSOCIATES LTD. (2008) – All Rights Reserved.

7.3 Phase analysis

The correlations of and phase difference between channels corresponding to different polarization were investigated. The correlation and phase difference between channels were calculated using a moving average with a window size of 5×5 pixels. (Different window sizes have not been tested in the present study.) The absolute values of correlation coefficients for ocean are calculated using the selected ocean area (range pixels 1000 to 1300 and azimuth pixels 1900 to 2600 in Figure 6a)) and the results are given in Table 3.

Table 3: Absolute correlation coefficients for ocean.

	HH	HV	VH	VV
HH	1.00	0.05	0.07	0.97
HV	0.05	1.00	0.46	0.04
VH	0.07	0.46	1.00	0.07
VV	0.97	0.04	0.07	1.00

The correlation of and phase difference between the HH and VV channels are shown in Figure 8 and 9 respectively. In the phase difference image (Figure 9), the phase angle is indicated in degrees in the colorbar.

From the results, we can see that the image of the ocean is highly correlated between HH and VV channels. This is consistent with our previous studies and results in the literature [13][20]. The high correlation of the ocean aids in observation of candidate targets, consequently it aids in discriminating the target and the “ghost” images. These “ghost” images in the range direction are due to the payload performance for high resolution modes. Since these data were acquired, MDA has implemented modifications to significantly reduce these “ghost” images. Two examples of “ghost” images are indicated in Figure 8.

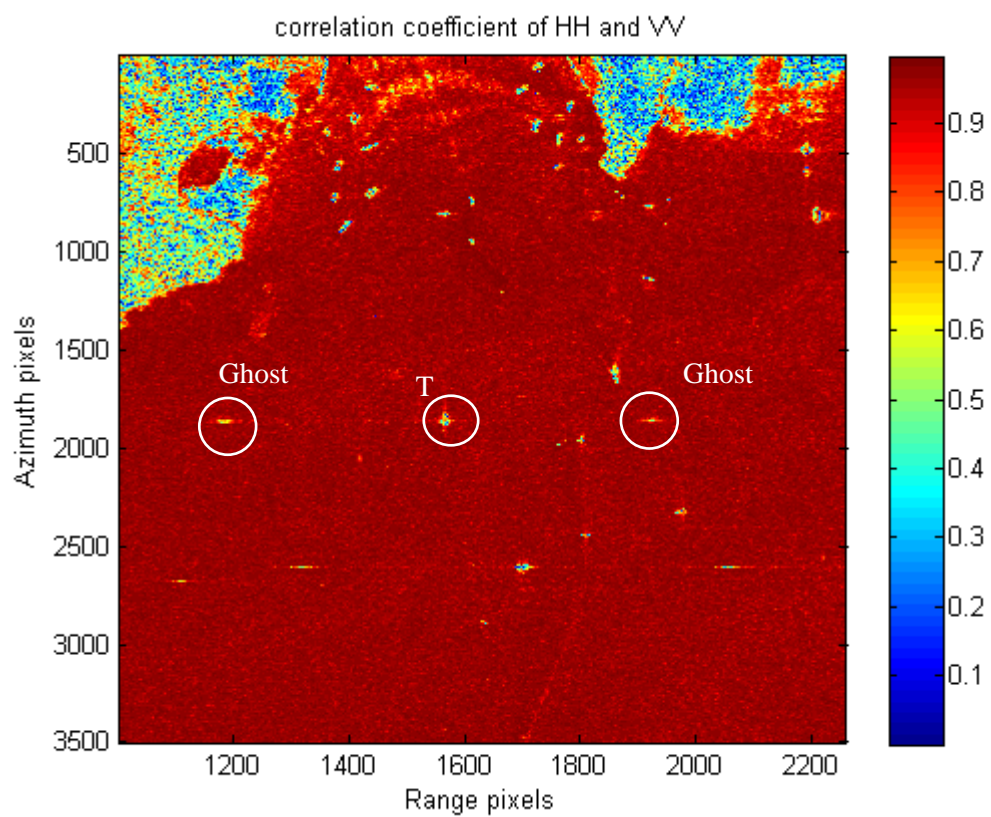


Figure 8: Correlation coefficient of HH and VV for test area.

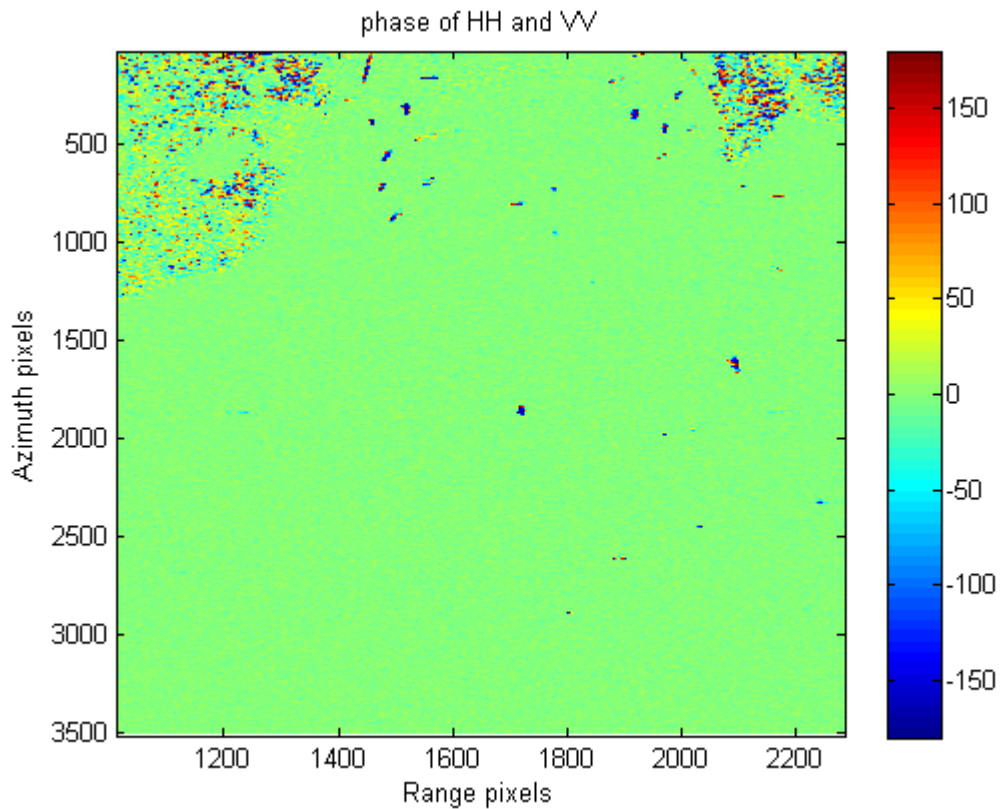


Figure 9: Phase difference between HH and VV for test area.

The correlation of and phase difference between the HV and VH channels are shown in Figure 10 and 11, respectively. These figures indicate that the targets are highly correlated, but the azimuth ambiguities have a phase difference of 180° , as expected [13]. As previously indicated, this phase difference between the HV and VH channels can be used to aid in distinguishing between targets and azimuth ambiguities.

Figure 12 gives examples of correlation of and phase difference for a few targets whose locations are indicated in Figure 7.

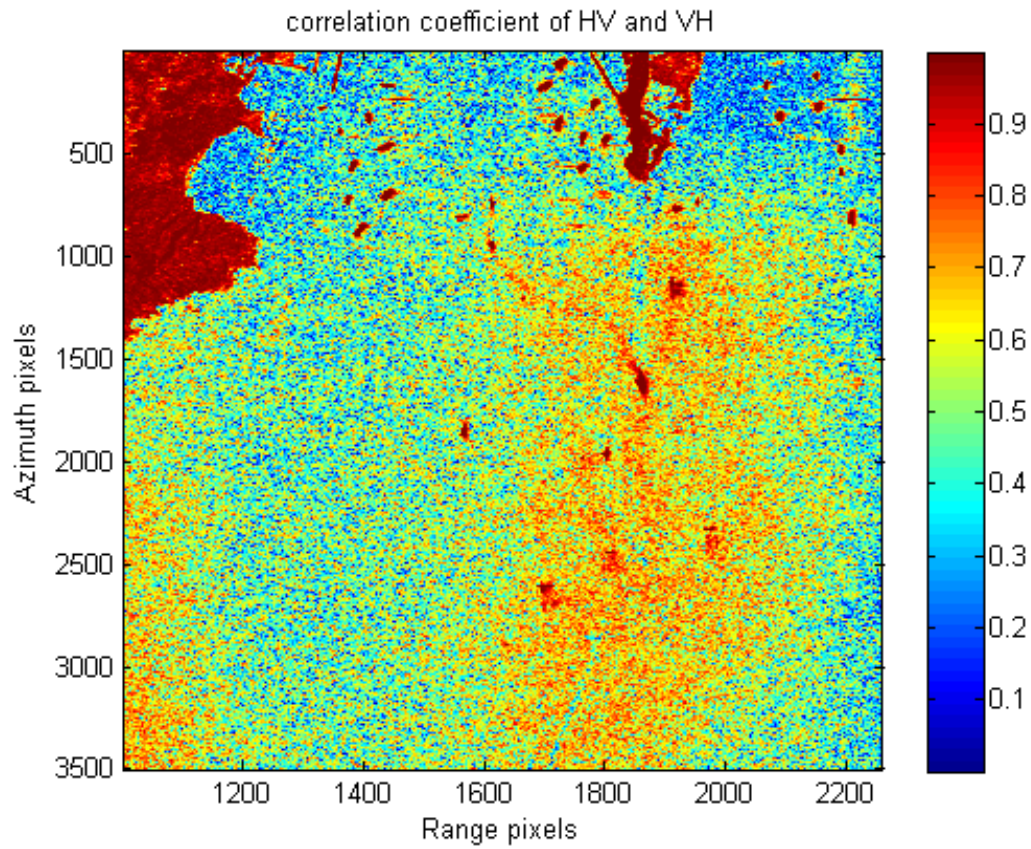


Figure 10: Correlation coefficient of HV and VH for test area.

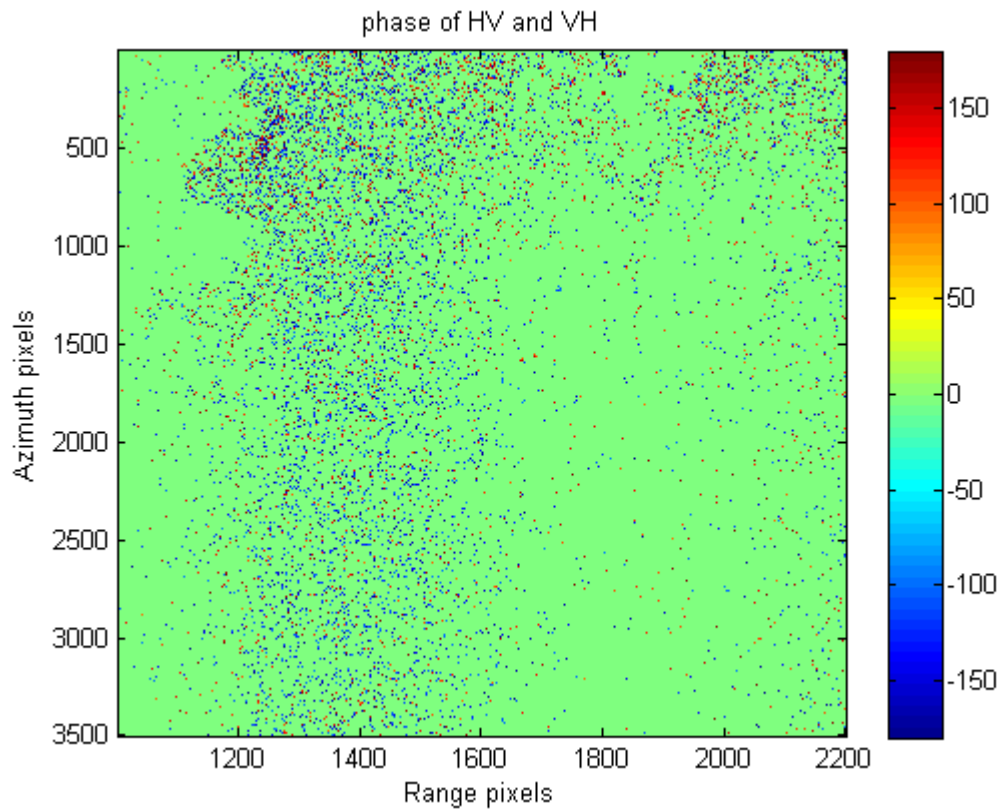


Figure 11: Phase difference between HV and VH for test area.

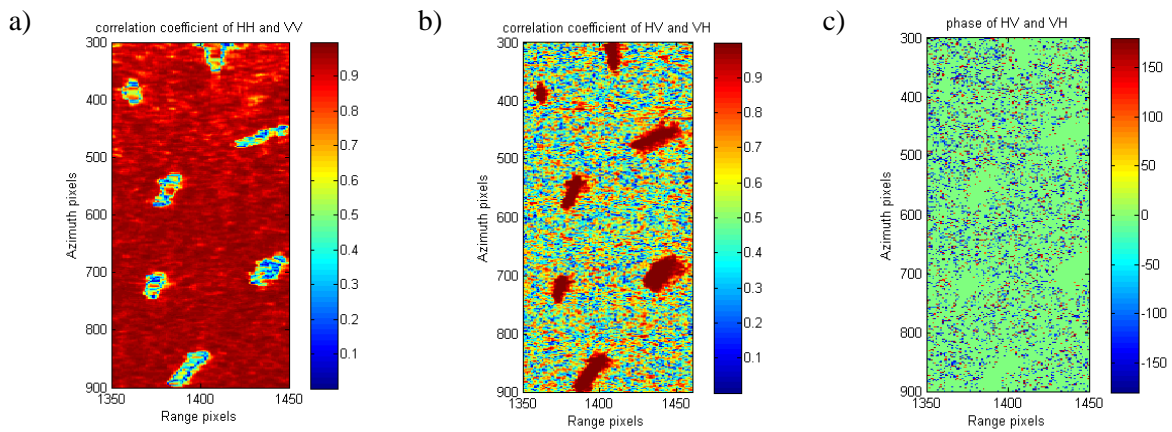


Figure 12: a) Correlation coefficient of HH and VV; b) correlation coefficient of HV and VH; c) phase difference between HV and VH.

The correlation of the HH and VV channels as shown in Figure 12a) indicates that the ocean is highly correlated, but targets are not. On the other hand, the correlation of HV and VH channels shown in Figure 12b) indicates that the targets are highly correlated, and the phase difference is approximately 180° , as shown in Figure 12c). The phase analysis results confirm that detected candidate targets are not processing artefacts. The signatures of some ships can be seen.

Figure 13a) shows the image of the correlation of the HV and VH channels of a target, Figure 13b) shows the phase difference between the HV and VH channels of the ambiguity of this target, and Figure 13c) shows the ambiguity of the target. This ambiguity was detected as a candidate target. However, it was distinguished from the actual targets by the phase analysis.

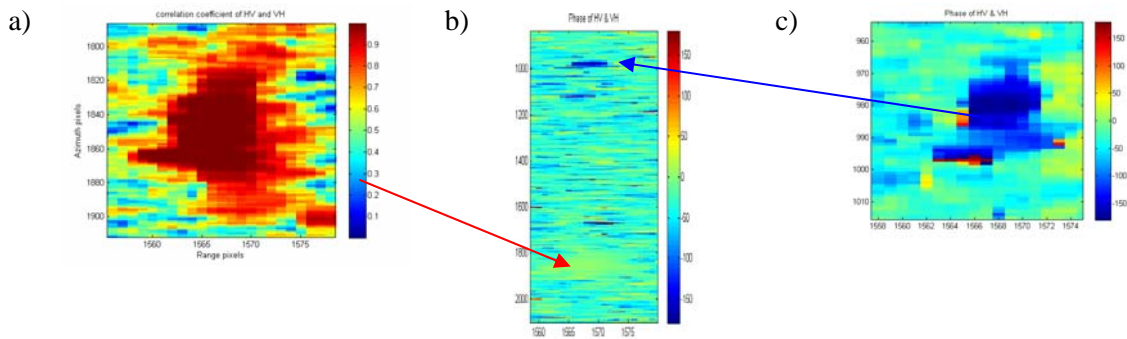


Figure 13: Example phase analysis results of HV and VH. a) correlation coefficient for a ship; b) phase difference for a target and an ambiguity; c) phase difference for an ambiguity.

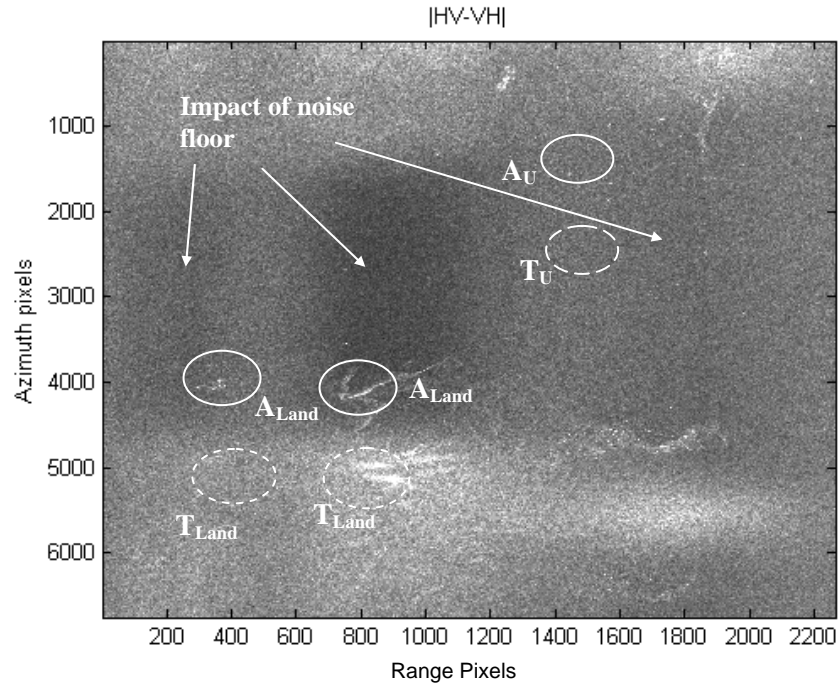
Azimuth ambiguities can also be clearly observed in the $|HV-VH|$ image. Based on the phase properties of HV and VH channels described in Section 3.3, when the $|HV-VH|$ image is formed, the amplitudes of the odd-order azimuth ambiguities are enhanced, while the amplitudes of the targets and even-order azimuth ambiguities are “cancelled”.

The $|HV-VH|$ image of the scene is shown in Figure 14a). Some azimuth ambiguities can be seen. Examples of ambiguities of regions on the land are indicated. In the $|HV-VH|$ image, the impact of the system noise floor higher than the signal is visible in the very low backscatter regions. To aid in observation of ambiguities in the $|HV-VH|$ image, the $|HV|$ image is also shown in Figure 14b).

According to Equation (3), the distance between the ambiguity A_U and the target T_U is estimated to be approximately 4.4 km. Similarly, the azimuth ambiguities (A_{land}) corresponding to the structures on the land which occur at smaller slant ranges are found to be displaced approximately 4.3 km from the actual position (T_{Land}). (See also Figure 13 for the target T_U and the ambiguity A_U .) The measurements from the images agree with these calculated values.

The results demonstrate that the quad-pol system provides improved ship detection and the phase information between HV and VH can be used to distinguish azimuth ambiguities and targets, consequently aiding in reducing the false alarm rate. The relative detection performance of various polarization combinations will be considered in Section 7.5.

a)



b)

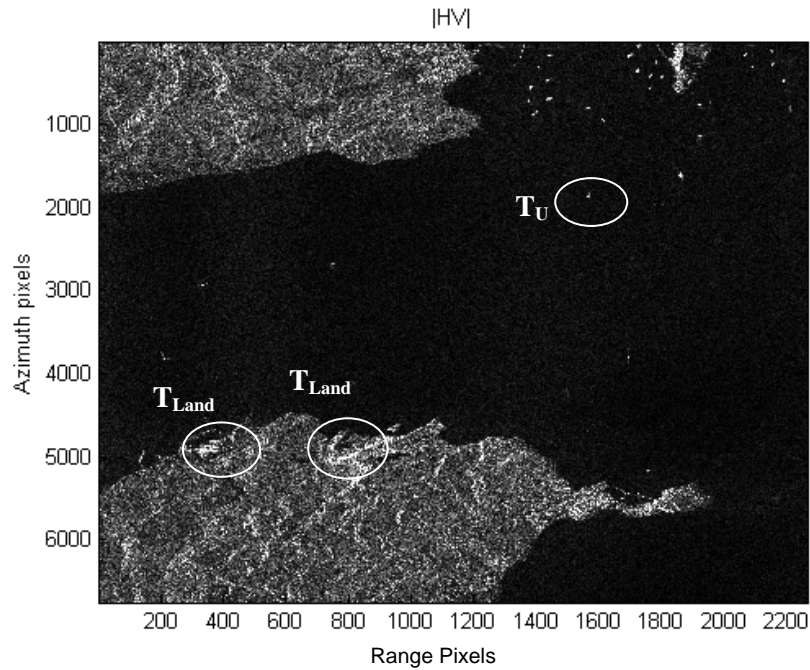


Figure 14: a) $|HV - VH|$; b) $|HV|$ image of the Strait of Gibraltar.

Original RADARSAT-2 Data and Products ©MacDonald, Dettwiler and Associates Ltd., 2008 – All Rights Reserved.

7.4 Compact PolSAR ship detection

The compact polarimetric SAR data were simulated using measured RADARSAT-2 FQ Mode data as described in Section 4.

The Likelihood Ratio Test Ship Detection software was applied to the simulated CL data. The detection threshold calculation procedures and the ocean sample area are the same as described in Section 7.2. The detection threshold is approximately 13.4 dB calculated with P_{FA} set to approximately 10^{-6} .

The detection results are shown in Figure 15. The results are similar to those from the quad-pol detection shown in Figure 7.

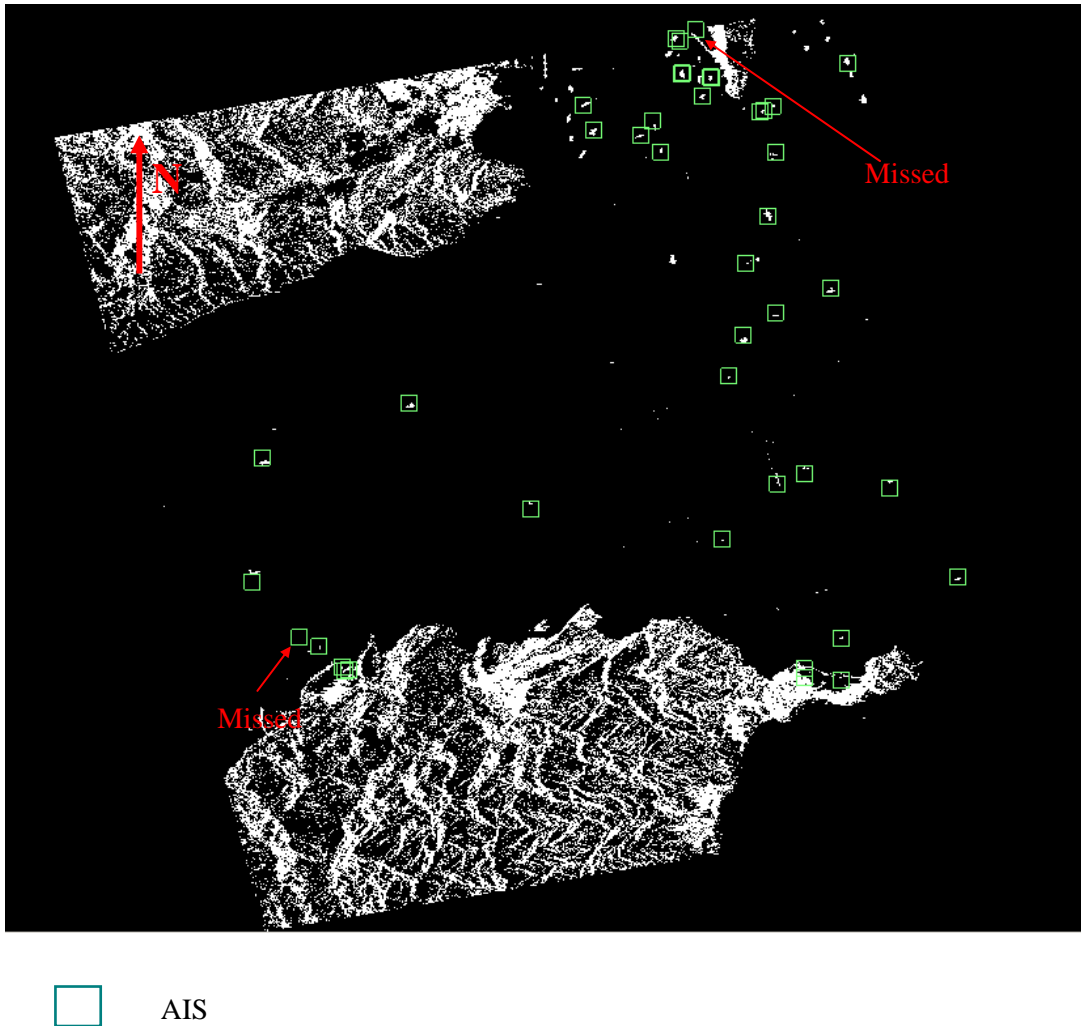


Figure 15: Detection results for simulated CL data of the Strait of Gibraltar in a geodetic projection.

7.5 Ship detection comparison

The ship detection performance for RADARSAT-2 FQ Mode data and the simulated CL data as well as dual-pol HH+HV amplitude only and single-pol HH have been examined and the ROC curves determined. The HH polarization is used as a baseline since this is the transmit-receive configuration for RADARSAT-1. The detection performance analysis was carried out for eight ships in the test scene. (See Table 2.)

As examples, the detection performance curves for ships 3 and 6, are presented in Figure 16a) and 17a), respectively, where b) and c) show the corresponding $|HH|$ and simulated $|X_1|$ images. Results for the other vessels are presented in Annex A.

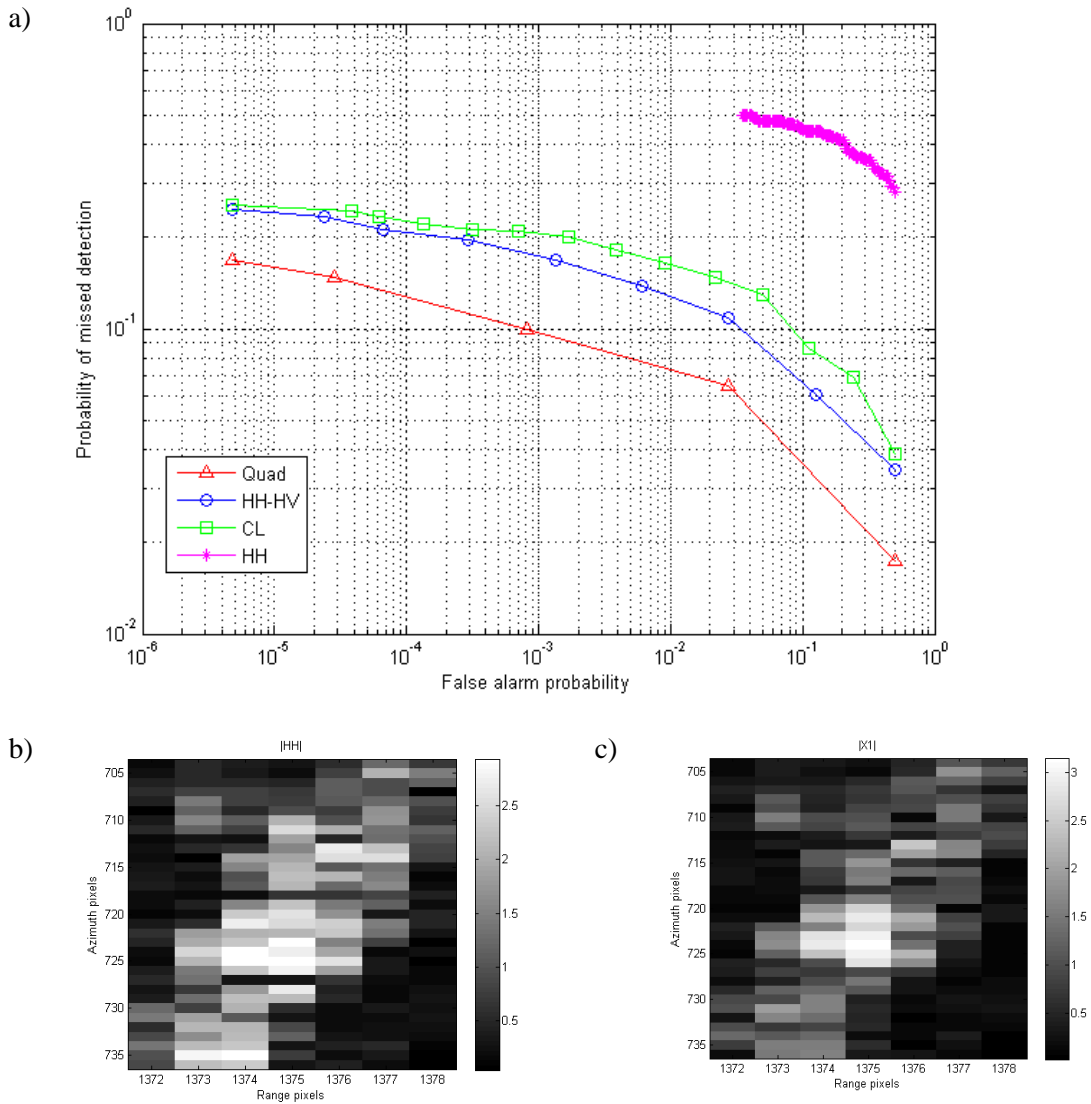


Figure 16: a) Detection performance for ship 3; b) $|HH|$ image and c) simulated $|X_1|$ image.

Original RADARSAT-2 Data and Products ©MacDonald, Dettwiler and Associates Ltd., 2008 – All Rights Reserved.

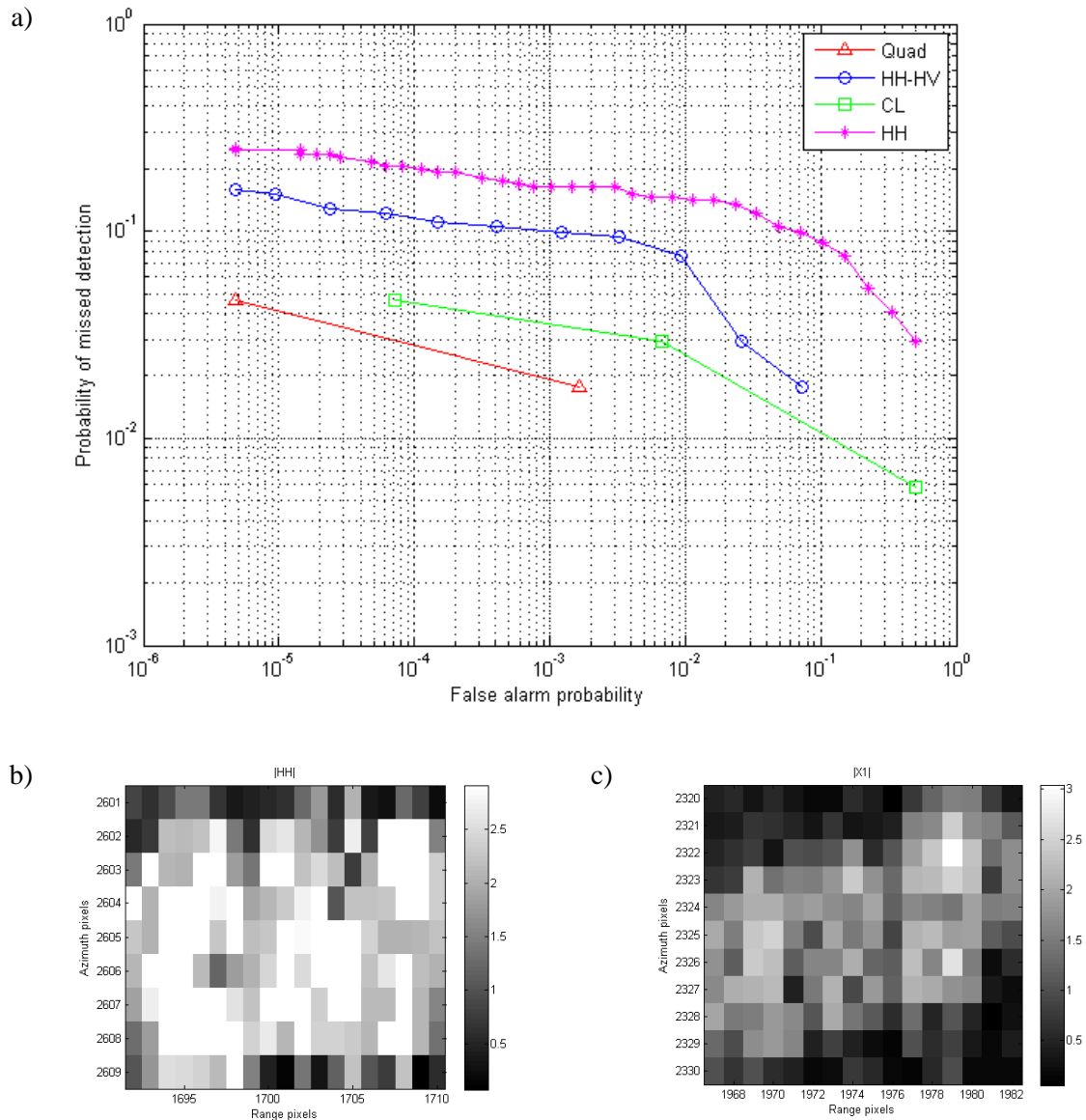


Figure 17: a) Detection performance for ship 6; b) $|HH|$ image and c) simulated $|X_1|$ image.

Original RADARSAT-2 Data and Products ©MacDonald, Dettwiler and Associates Ltd., 2008 – All Rights Reserved.

In general, a lower P_{FA} results in a higher P_{MD} , or a lower P_{MD} results in a higher P_{FA} . A system having the lowest P_{FA} and lowest P_{MD} provides the best detection, i.e. the lower the curve, the better the performance. Thus, all of these ROC curves clearly show the advantage (i.e., decreased probability of missed detection, decreased probability of false alarm) of a quad polarization

system, which uses all of the available amplitude and phase information (triangles). Dual polarization systems with amplitude only provide much better performance than single channel HH polarization (asterisks).

For five of eight cases studied, the simulated CL data (square) provide better performance than HH + HV with amplitude only (circles). For the other three cases, HH + HV with amplitude only provides slightly better performance than the simulated CL system.

By arbitrarily selecting a probability of false alarm of $P_{FA} = 10^{-4}$, the relative improvement in ship detectability may be quantified by comparing the probabilities of missed detection P_{MD} . The relative improvement in the detection performance of all cases studied is summarized in Table 4 by taking the ratio of the observed P_{MD} to that of quad polarization P_{MD}^Q . We observed that an approximately seven-fold decrease in the probability of missed detection was achieved by moving from a single polarization to a polarimetric radar system, and a four-fold decrease by moving to a simulated CL system. In some cases, the single channel system cannot provide such low probability of missed detection. (See Figure 16a.) These results show that a quad polarization system provides the best detection for the cases studied, but a CL system will provide much better performance than a single channel radar system.

A statistical analysis of the detection performance of these systems was performed. The mean value and the standard deviation of the mean of each system were calculated on the observed P_{MD} values. The mean values of the P_{MD} and the standard deviation of the mean values are normalized to those of the HH system.

The uncertainty in the normalized mean of the P_{MD} is given by:

$$\delta C = \sqrt{\left(\frac{1}{b} \times \delta a\right)^2 + \left(\frac{a}{b^2} \times \delta b\right)^2} \quad (8)$$

where a is the mean of individual system, δa is the corresponding standard deviation, b is the mean of HH system and δb is the corresponding standard deviation. These results are summarized in Table 5.

Table 4: Values of P_{MD} for $P_{FA} = 10^{-4}$ for ships considered.

Ship ID #	System	P_{MD}	P_{MD}/P_{MD}^Q
1	HH	—	—
	HH+HV	2.0×10^{-1}	2.00
	CL	1.5×10^{-1}	1.50
	Quad-pol	1.0×10^{-1}	1.00
3	HH	—	—
	HH+HV	2.1×10^{-1}	1.50
	CL	2.2×10^{-1}	1.57
	Quad-pol	1.4×10^{-1}	1.00
4	HH	—	—
	HH+HV	2.5×10^{-1}	1.25
	CL	3.0×10^{-1}	1.50
	Quad-pol	2.0×10^{-1}	1.00
6	HH	2.0×10^{-1}	6.90
	HH+HV	1.1×10^{-1}	3.79
	CL	4.6×10^{-2}	1.59
	Quad-pol	2.9×10^{-2}	1.00
7	HH	4.3×10^{-1}	6.18
	HH+HV	2.0×10^{-1}	2.99
	CL	1.0×10^{-1}	1.49
	Quad-pol	6.7×10^{-2}	1.00
8	HH	—	—
	HH+HV	1.5×10^{-1}	1.36
	CL	1.9×10^{-1}	1.73
	Quad-pol	1.1×10^{-1}	1.00
9	HH	4.0×10^{-1}	4.08
	HH+HV	2.9×10^{-1}	2.96
	CL	1.3×10^{-1}	1.33
	Quad-pol	9.8×10^{-2}	1.00
10	HH	—	—
	HH+HV	3.2×10^{-1}	2.91
	CL	1.4×10^{-1}	1.23
	Quad-pol	1.1×10^{-1}	1.00

Table 5: Statistical analysis results of detection performance for $P_{FA} = 10^{-4}$.

	Mean (P_{MD})	std of mean	C (Mean/Mean ^{HH}) $\pm \delta C$
HH	0.34	0.07	1.00 ± 0.30
HH+HV	0.22	0.02	0.63 ± 0.15
CL	0.16	0.03	0.46 ± 0.13
Quad-pol	0.11	0.02	0.31 ± 0.08

The normalized values of the mean of the P_{MD} for the quad polarization, simulated CL and HH+HV systems demonstrate, from another perspective, that a quad polarization system provides a significant decrease of the probability of missed detection from that for a single polarization, while a CL system will achieve much lower probability of missed detection than a single channel system.

A compact polarimetric system should be capable of wider swath than conventional polarimetry having similar resolution since it only stores half of the data volume per pixel. Such a system is expected to provide better detection performance than a conventional dual polarization system. However, more investigation is required to verify this expectation. In contrast, a CL system could provide higher resolution than the quad polarization system while maintaining similar swath coverage.

8 KCFAR ship detection

Previous sections described the detection performance of the quad-pol ship detection algorithms based on the likelihood ratio test, developed using airborne PolSAR data to the RADARSAT-2 FQ data. Further optimization of these algorithms has been carried out. The optimization, implementation of optimized algorithms and initial detection results are presented in this section.

8.1 Estimation of K-distribution parameters for quad-pol data

In order to improve the quad-pol ship detection described in Sections 3.3, the probability density function (PDF) of the ocean decision variable has been studied.

The K-distribution for ocean samples of a SAR image can be described as [18][22]:

$$p(I) = \frac{2}{I} \left(\frac{L\nu I}{\langle I \rangle} \right)^{\frac{L+\nu}{2}} \frac{1}{\Gamma(L)\Gamma(\nu)} K_{\nu-L} \left(2\sqrt{\frac{L\nu I}{\langle I \rangle}} \right) \quad (9)$$

where $p(I)$ is the probability of image intensity I , $\langle I \rangle$ is the mean intensity, L is the equivalent number of statistically independent looks (ENL) in the scene, ν is the order parameter and describes the local modulation of the mean due to geophysical processes such as winds, waves, and currents, Γ is the gamma function, and $K_{\nu-L}$ is the modified Bessel function of the second kind of order $\nu - L$. L and ν define the shape of the K-distribution, which in turn are used in the threshold calculation for pixel-based ship detection in a CFAR detector.

In the quad-pol ship detector, the image intensity I is the decision variable calculated using Equation (2).

In general, ENL is a SAR processor characteristic. However, for the decision variable, which is derived from the combination of four channels of single-look products, the number of looks L is unknown. Also, the order number ν is unknown. The approach which we have taken to estimate these two parameters is as follows.

First, we choose a value for L then estimate ν , then plot the K-distributed PDF for each pair of L and ν , then test how well the estimated K-distribution function fits the measured data. Two methods were used; one is the root mean square error and the other is the χ^2 goodness-of-fit test. If the tests from both methods agree well, then the L and ν are found acceptable. The L is varied from 1 to 8. For each L , ν is varied from 1 to 200. The increment of L is 0.05 between $L = 3.8$ to 4.1, and 1 for others. For the ocean samples which we used for the test, it was found that L is 4 and ν is 40.95.

The histogram of the K-distributed ocean decision variable and the continuous PDF according to Equation (9) are shown in Figure 18. The results indicate that the K-distribution is a good model for the ocean decision variable from the combination of four channels.

Therefore, the detection algorithms based on the likelihood ratio test have been optimized and the decision variable has been input into a KCFAR detector. The KCFAR detector used was one developed by Dstl in ADSS [19]: the algorithms for deriving the decision variable for quad polarization data was developed by DRDC Ottawa and it produced the image input to the KCFAR detector.

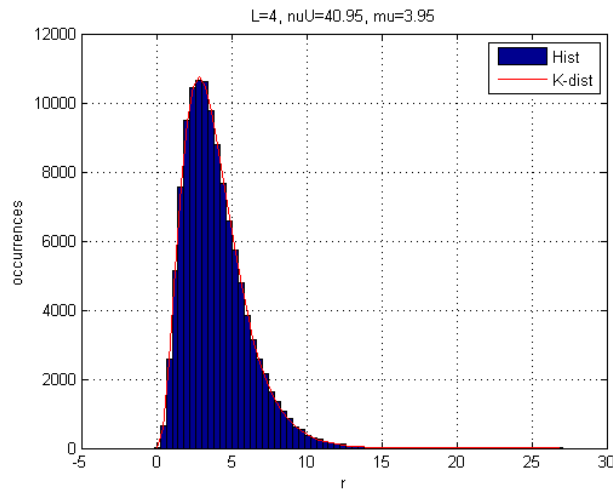


Figure 18: Probability density function of the ocean decision variable.

8.2 Operation of the KCFAR detector

After implementation of the detection algorithms using ADSS, tests were performed on the test image.

In order to avoid significant variation of ocean statistics over large areas in an image, the decision variable is calculated on a small area (tile) basis. The entire scene is divided into small tiles: i.e. 10×10 tiles for FQ images since the coverage is only 25×25 km.

In order to eliminate the effect of ocean pixels with high decision variable values, the ocean sample median of $|HH|^2$ and the median of $|HV|^2$ were calculated, then the $|HH|^2$ and $|HV|^2$ values of each ocean pixel are compared to these medians. If the intensity of each pixel meets the condition of ($|HH|^2 < 5 \times \text{median } |HH|^2$ and $|HV|^2 < 5 \times \text{median } |HV|^2$), then the pixel will be used to calculate the decision variable.

The decision variable for each pixel in an image is calculated and sent to the KCFAR detector (KCFAR_Quad) as the required parameter to perform the pixel detection.

The straightforward processing chain is to land mask the images, run the KCFAR_Quad algorithms, cluster the results into candidate targets, and display the results in IA Pro.

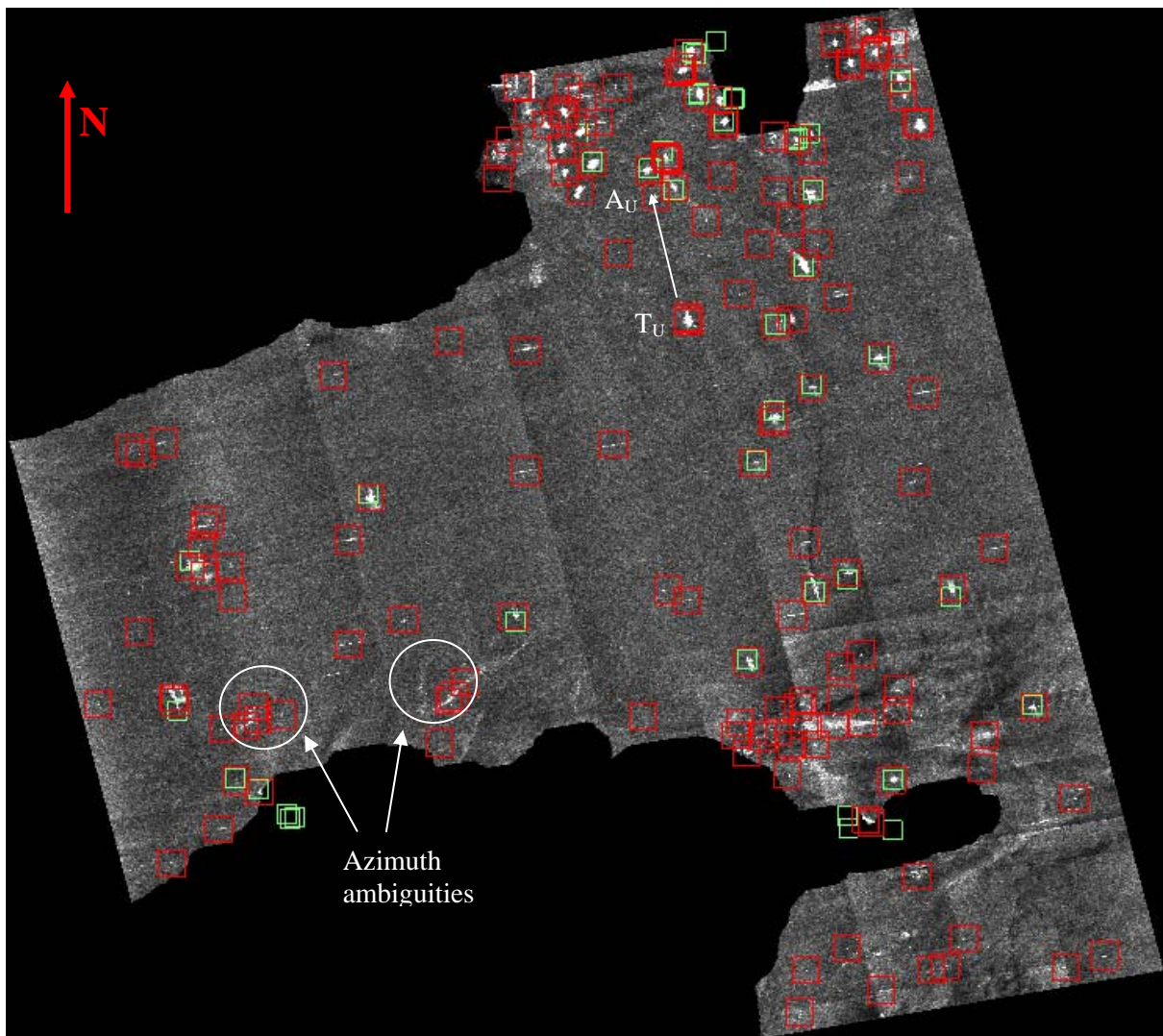
The KCFAR algorithm in ADSS sets a guard region and an annulus in estimating the K-distribution parameters of the background without contamination from potential target pixels. Several sets of values for the annulus parameters were tried to determine the behaviour of the algorithm. Those values were chosen to maximize the detection of targets declared on the basis of AIS data and the visual evaluation.

For this study, $P_{FA} = 10^{-10}$ is used. Other parameters, including multi-look, correlation and clutter estimation method, are set to default values.

8.3 Initial detection results

Initial detection results from the KCFAR_Quad detector are illustrated in Figure 19. The image (acquired on 29 July 2008) is the same as used in earlier studies described in this report. This image shows the decision variable image with a land mask based on the World Vector Shoreline (WVS) applied. Detection results are indicated as red squares while the AIS results are green squares. Thirty-six ships were declared by the AIS. Two-hundred-forty candidate targets were declared by the KCFAR_Quad, including 30 ships declared by the AIS. The smallest ship declared by both AIS and the KCFAR_Quad detectors had a length of 18 m. It is noted that six of the ships declared by the AIS appear to have been eliminated by application of the land mask.

Some azimuth ambiguities were detected as candidate targets. The azimuth ambiguities can be distinguished from the targets according to Equation (3) in section 3.3. Examples of azimuth ambiguities which were detected as candidate targets are shown in Figure 19 (the decision variable image). However, these azimuth ambiguities were distinguished from the actual targets, as shown in Figure 20 (the HH image), which zooms in on the areas of interest. The detection results are the red squares, the targets are green rectangles and the ambiguities are yellow rectangles. These initial results demonstrate that small ships are more likely to be detected using the KCFAR_Quad detector.



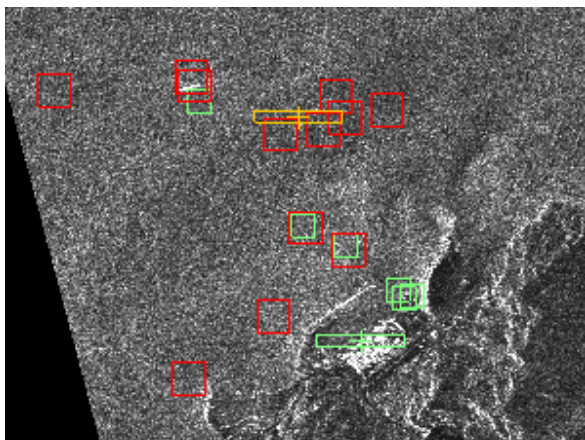
KCFAR_Quad

AIS

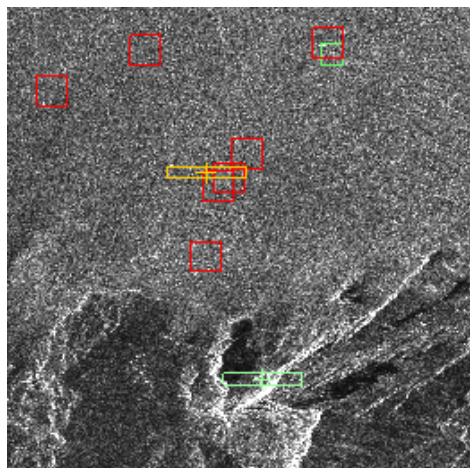
Figure 19: KCFAR detection results of the Strait of Gibraltar in a geodetic projection.

Original RADARSAT-2 Data and Products ©MacDonald, Dettwiler and Associates Ltd., 2008 – All Rights Reserved.

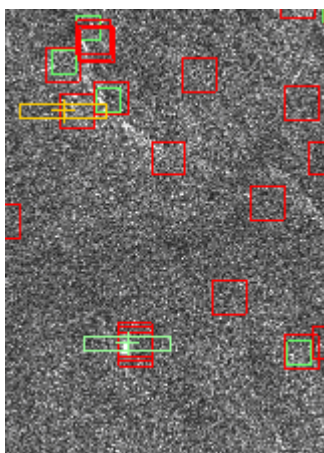
a)




b)



c)



 Target

 Azimuth ambiguity

 KCFAR_Quad

 AIS

Figure 20: KCFAR detection results. a) and b) land ambiguities; c) a target and its ambiguity.

Original RADARSAT-2 Data and Products ©MacDonald, Dettwiler and Associates Ltd., 2008
– All Rights Reserved.

9 Conclusions

This study has evaluated the baseline performance of ship detection algorithms applied to RADARSAT-2 FQ data. The algorithms were originally developed using airborne PolSAR images from the CV-580 system and this study verifies that the same algorithms, which are based on the likelihood ratio test, are applicable to RADARSAT-2 images as well.

Ship detection performance for various SAR systems, including quad polarization, HH + HV with amplitude only, and single polarization HH has been estimated. In addition, a CP, right circular transmit and linear receive, SAR system was simulated using measured data from RADARSAT-2 FQ Mode. The polarimetric SAR ship detection algorithms were also applied to this CP system.

It has been shown that when a CP system is simulated using RADARSAT-2 FQ data, the noise power in each CP channel is twice the noise power in each RADARSAT-2 channel. However, the two channels of the CP system are dominated by the co-polarization channels of the RADARSAT-2 image. Since the ocean clutter of the co-polarization channels is about 30 dB above the noise floor, the effective target to clutter ratio will be affected only slightly by the thermal noise floor. The system performance is approximately determined by the effective target to clutter ratio of the signal components. Therefore, the effect of the RADARSAT-2 system noise on the simulated CP system detection performance can be ignored.

The quad polarization system provides the best detection in this application; the dual polarization systems, simulated CP and HH + HV with amplitude only, provide better detection than single channel systems. For five of the test targets studied, the CP SAR system provides significantly better detection than the HH + HV amplitude only system. For the other three cases, the HH + VH system provides slightly better detection than the CP system. It is judged that the CP system is better than the HH + HV amplitude only system. The CP SAR system therefore has potential for improved ship detection. At the same time, a dual polarization system will have wider swath coverage than that of a quad polarization system having the same resolution.

It was also verified that the phase difference between the HV and the VH channels can aid in distinguishing targets and azimuth ambiguities, consequently, reducing the false alarm rate.

The new KCFAR ship detector (KCFAR_Quad) based on feeding the PolSAR decision variable derived from the likelihood ratio test into a KCFAR detector, has been tested. The algorithms for calculating the decision variable from quad polarization data was implemented as the required parameter of the KCFAR detector in ADSS. The initial results demonstrate the applications of this detector for ship detection with quad polarization data.

The RADARSAT Constellation Mission will provide CP SAR as an operational mode. It is recommended that this mode be considered for wide area surveillance since it will provide wider swath coverage than quad-pol mode, yet it has additional phase information which conventional dual polarization does not have. The phase information will aid in improving ship detection to reduce the probability of false alarms.

References

- [1] Liu, C., Vachon, P.W. and Geling, G.W. (2005). Improved ship detection with airborne polarimetric SAR data. *Canadian Journal of Remote Sensing*, 31(1), 122-131.
- [2] Scharf, L.L. (1991). Statistical signal processing – Detection, estimation, and time series analysis. Addison-Wesley Publishing Company, Inc.
- [3] Redding, N.J., Kettler, D.I., Blucher, G., and Perry, P.G. (2003). The Analysts' Detection Support System for deploying a network of target detection and recognition algorithms in SAR exploitation. Proc. 2003 International Conference on Radar, 3-5 Sept. 2003, Adelaide, Australia, Cooperative Research Centre for Sensor Signal and Information Processing and IEEE South Australia Section, 448-453. CD-ROM Proceedings.
- [4] Raney, R.K. (2007). Hybrid-polarity SAR architecture. *IEEE Transactions on Geoscience and Remote Sensing*, 45(11), 3397-3404.
- [5] Vachon, P.W., English R.A. and Wolfe J. (2007). Ship signatures in RADARSAT-1 ScanSAR Narrow B imagery: Analysis with AISLive data. DRDC Ottawa TM 2007-052, Defence R&D Canada – Ottawa.
- [6] Souyris, J.-C., Imbo, P., Fjørtoft, R., Mingot, S. and Lee, J.-L. (2005). Compact polarimetry based on symmetry properties of geophysical media: the $\pi/4$ mode. *IEEE Transactions on Geoscience and Remote Sensing*, 43(3), 634-646.
- [7] Touzi, R (2009). Compact versus full polarimetric SAR. In Proceedings *PolInSAR Workshop*, Frascati, Italy. 26-30 January 2009. URL: http://earth.esa.int/workshops/polinsar2009/participants/525/pres_2_touzi_525.pdf [Accessed: 28 May 2009].
- [8] MDA, RADARSAT-2 (Online) (2009). <http://www.radarsat2.info/>. [Accessed: 11 Jan. 2009].
- [9] Canadian Space Agency (Online) (2009). <http://www.asc-csa.gc.ca/eng/satellites/radarsat2/default.asp>. [Accessed: 6 October 2009].
- [10] Cloude, S.R. and Pottier, E. (1996). A review of target decomposition theorems in radar polarimetry. *IEEE Transactions on Geoscience and Remote Sensing*, 34(2), 498-518.
- [11] Liu, C. and Meek, A. (2005). Likelihood ratio test polarimetric SAR ship detection application. DRDC Ottawa TM 2005-243, Defence R&D Canada – Ottawa.
- [12] Curlander, J.C. and McDonough, R.N. (1991). Synthetic aperture radar – systems and signal processing. John Wiley & Sons, Inc.

- [13] Liu, C. and Gierull, C.H. (2007). A new application of PolSAR imagery in the field of moving target indication/ship detection. *IEEE Transactions on Geoscience and Remote Sensing*, 45(11), 3426-3436.
- [14] Raney, R.K. and Princz, G.J. (1987). Reconsideration of azimuth ambiguities in SAR. *IEEE Transactions on Geoscience and Remote Sensing*, GE-25(6), 783-787.
- [15] Nord, M.E., Ainsworth, T.L., Lee J.-S. and Stacy, N.J.S. (2009). Comparison of compact polarimetric synthetic aperture radar modes. *IEEE Transactions on Geoscience and Remote Sensing*, 47(1), 174-188.
- [16] Raney, R.K. (2009). Hybrid-polarity SAR architecture. In *Proceedings PolInSAR Workshop*, Frascati, Italy. 26-30 January 2009. URL: http://earth.esa.int/workshops/polinsar2009/participants/141/pres_1_Raney_141.pdf [Last accessed: 28 May 2009].
- [17] Secker, J. and Vachon, P.W. (2007). Exploitation of multi-temporal SAR and EO satellite imagery for geospatial intelligence. In *Proceedings of the Fusion 2007 Conference*, 9-12 July 2007, Quebec City.
- [18] Blucher, G., Blacknell, D., Redding, N.J., and Vagg, D. (2003). Prescreening algorithm assessment within the Analysts' Detection Support System. Proc. 2003 International Conference on Radar, 3-5 September 2003, Adelaide, Australia, Cooperative Research Centre for Sensor Signal and Information Processing and IEEE South Australia Section, 454-459. CD-ROM Proceedings.
- [19] Redding, N.J., Blucher, G., Booth, D.M., Perry, P.G., Jones, R. and Hanan, R. (2004). The Analysts' Detection Support System: Architecture design and algorithms. Part 2—Algorithms. Intelligence, Surveillance and Reconnaissance Division, Information Sciences Laboratory, DSTO-TN-0522, March 2004.
- [20] International Maritime Organization (Online) (2009). http://www.imo.org/Safety/mainframe.asp?topic_id=754 [Last accessed: 6 October 2009].
- [21] Lee, J.-S., Hoppel, K.W., and Mango, S.A. (1994). Intensity and phase statistics of multilook polarimetric and interferometric SAR imagery. *IEEE Transactions on Geoscience and Remote Sensing*, 32(5), 1017-1028.
- [22] Wackerman, C.C., Pichel, W., Li, X. and Jackson, C. (2006). Toward an automated ship and wake detection system. In *Proceedings OceanSAR 2006 – Third Workshop on Coastal and Marine Applications of SAR*. St. John's, NL, Canada. October 2006. http://www.oceansar2006.com/papers/59_Wackerman_Oceansar2006.pdf

This page intentionally left blank.

Annex A Detection performance

The detection performance of data obtained from RADARSAT-2 FQ Mode as well as the simulated CL data have been studied, and the ROC curves determined. The detection performance analysis has been discussed in Section 7.5 and the comparison of the performance of various systems has been listed in Table 4. This Annex presents additional ROC curves. Figures a) present the ROC curves, Figures b) are the images of the $|HH|$ channel and Figures c) are the images of the $|X1|$ component of the simulated CL data. The results shown in this annex and in Section 7.5 clearly demonstrate that a quad polarization system (triangles) provides the best detection for the cases studied. A dual polarization system, the HH+HV amplitude only system (circles) and the simulated CP data (squares) provide better detection than a system operating in a single HH polarization (asterisks). For five of eight cases studied, the simulated CL data provides better performance than the HH+HV amplitude only system. For other three cases, the HH+HV with amplitude only system provides slightly better performance than the simulated CL data.

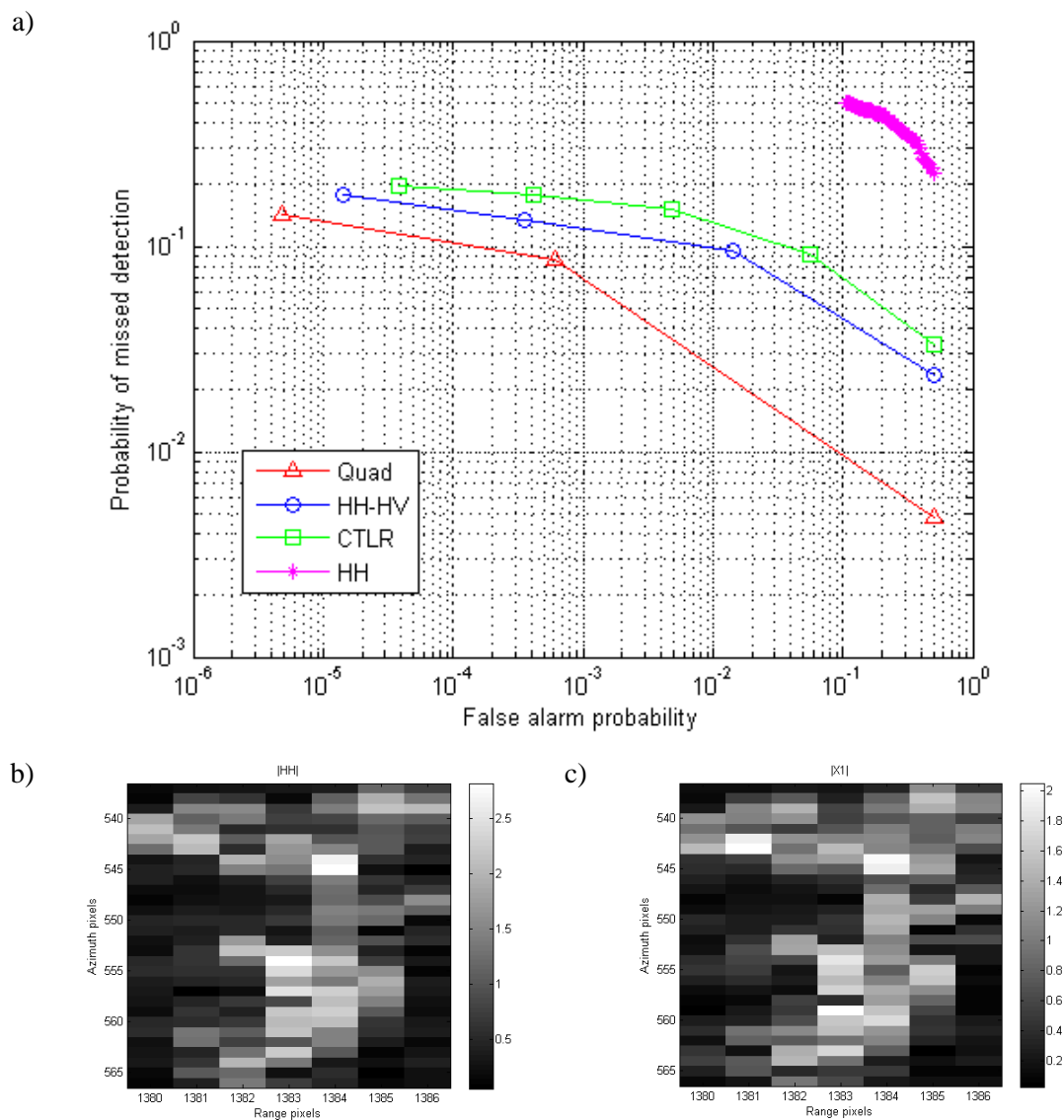


Figure 21: a) Detection performance for ship 1; b) $|HH|$ image and c) simulated $|X_1|$ image.

Original RADARSAT-2 Data and Products ©MacDonald, Dettwiler and Associates Ltd., 2008 – All Rights Reserved.

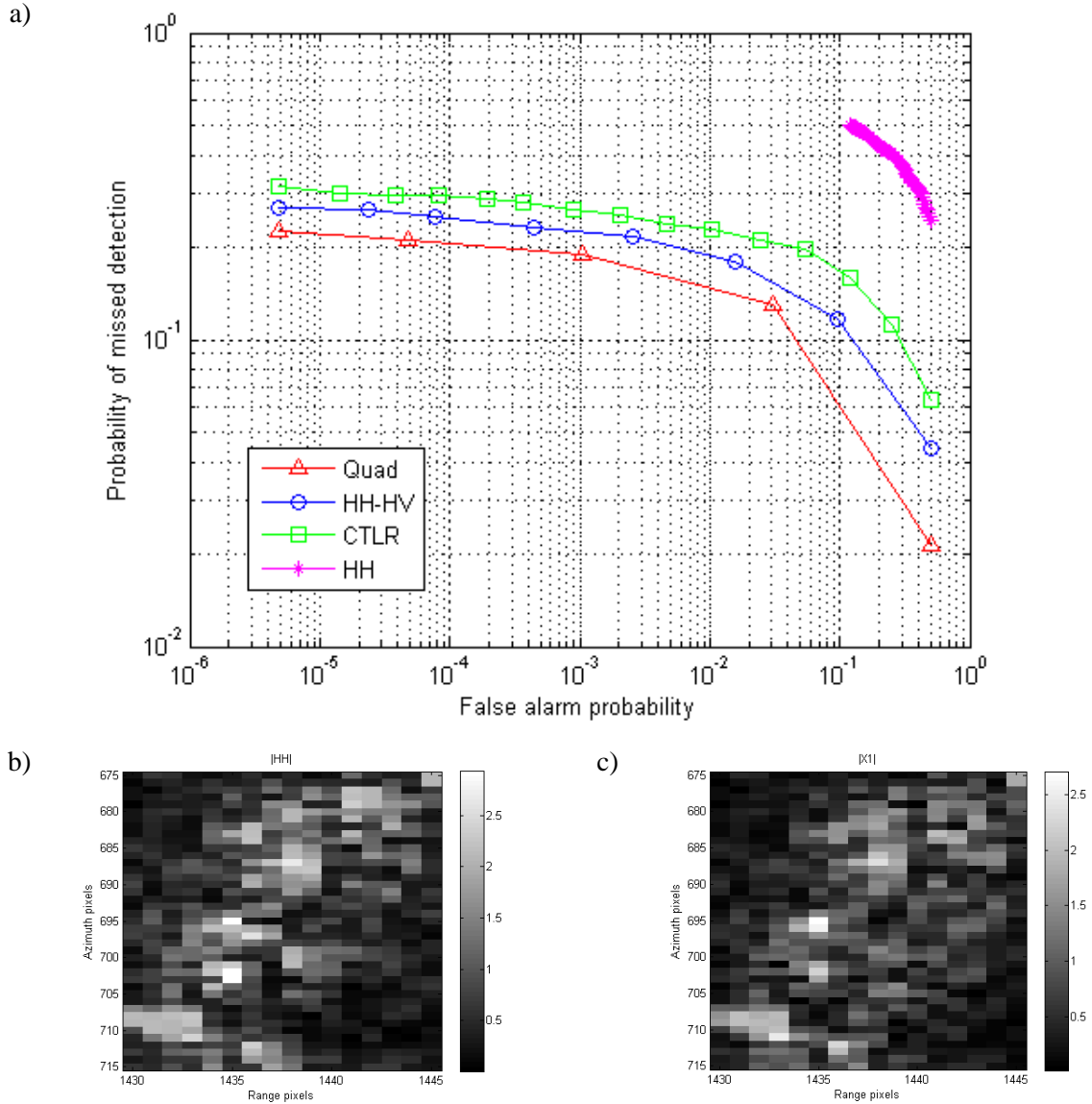


Figure 22: a) Detection performance for ship 4; b) $|HH|$ image and c) simulated $|X_1|$ image.

Original RADARSAT-2 Data and Products ©MacDonald, Dettwiler and Associates Ltd.,
2008 – All Rights Reserved.

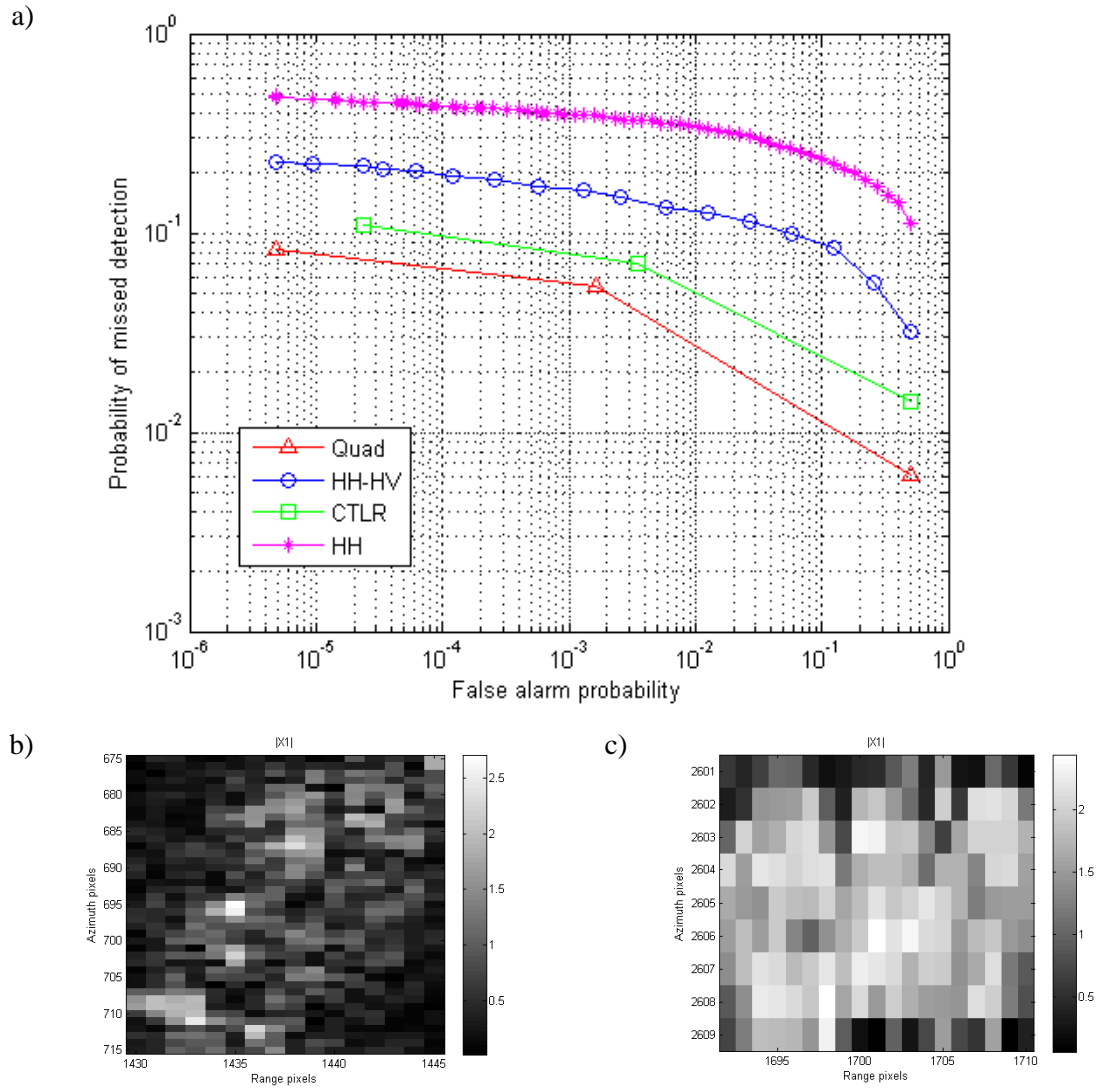
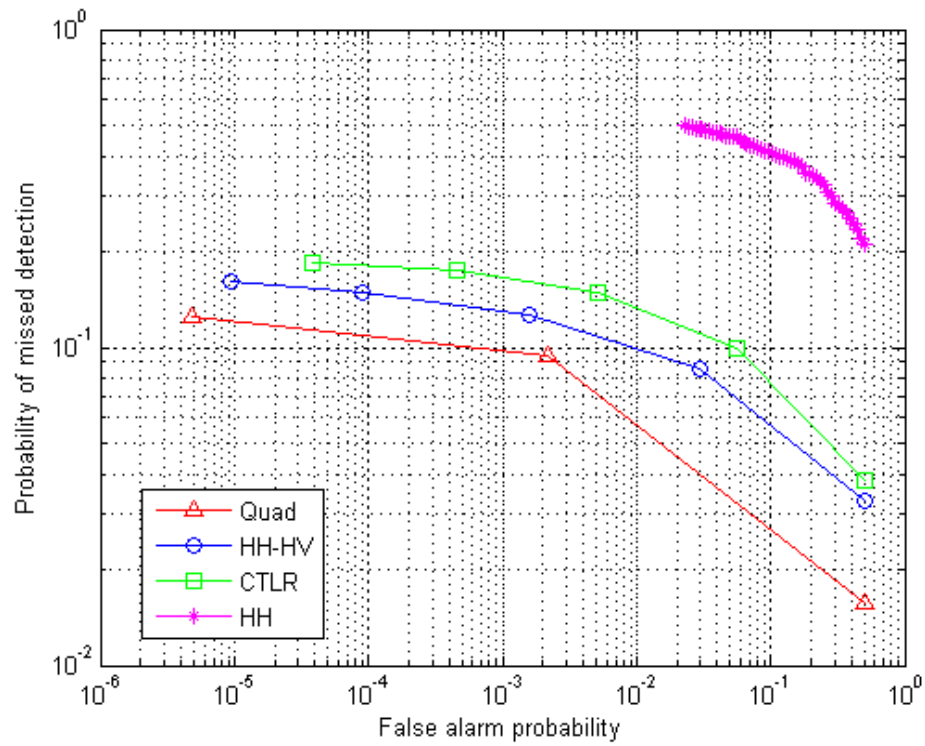


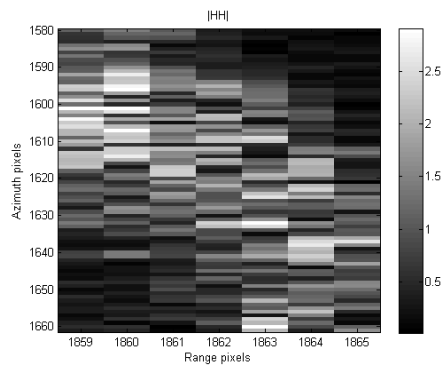
Figure 23: a) Detection performance for ship 7; b) $|HH|$ image and c) simulated $|X_1|$ image.

Original RADARSAT-2 Data and Products ©MacDonald, Dettwiler and Associates Ltd., 2008 – All Rights Reserved.

a)



b)



c)

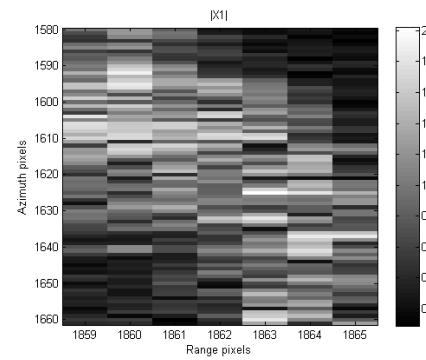
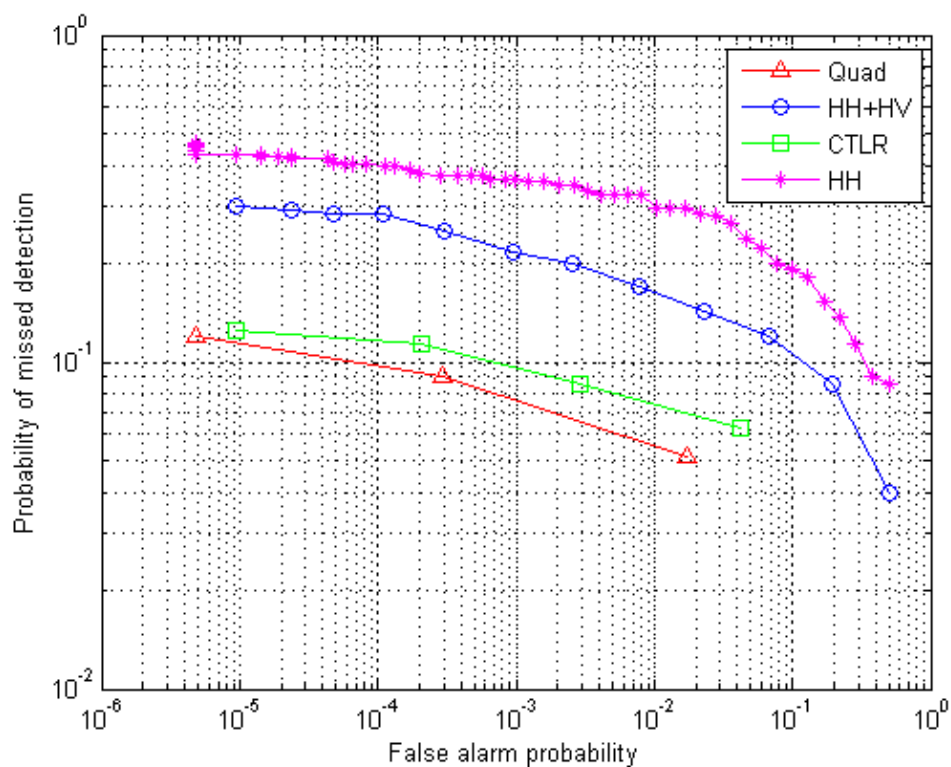


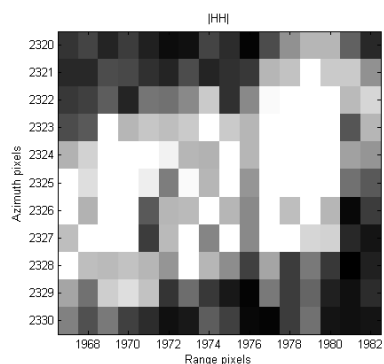
Figure 24: a) Detection performance for ship 8; b) $|HH|$ image and c) simulated $|X_1|$ image.

Original RADARSAT-2 Data and Products ©MacDonald, Dettwiler and Associates Ltd., 2008 – All Rights Reserved.

a)



b)



c)

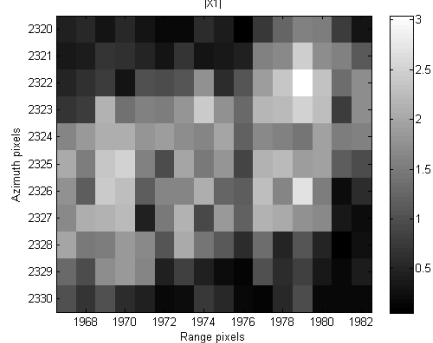
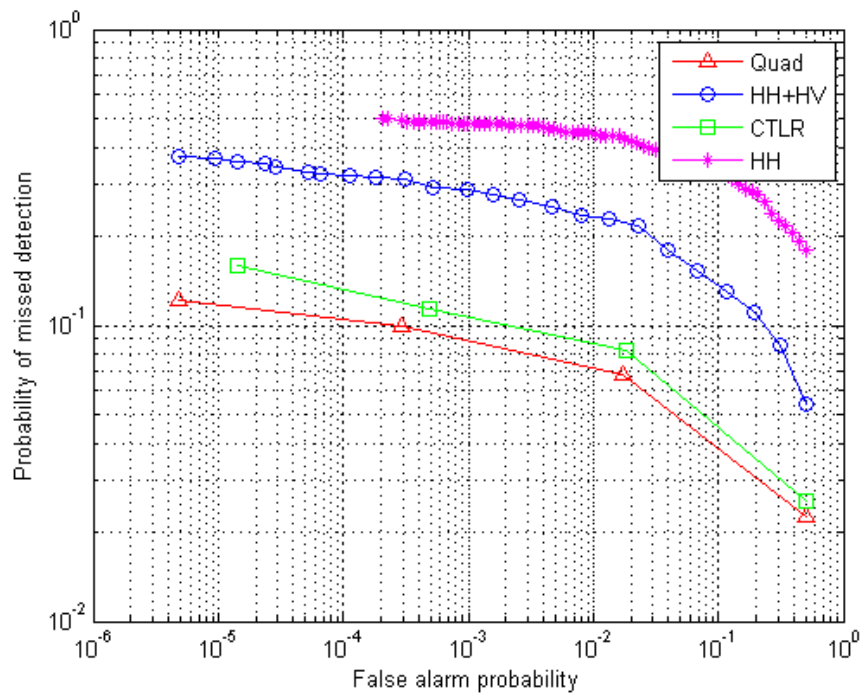


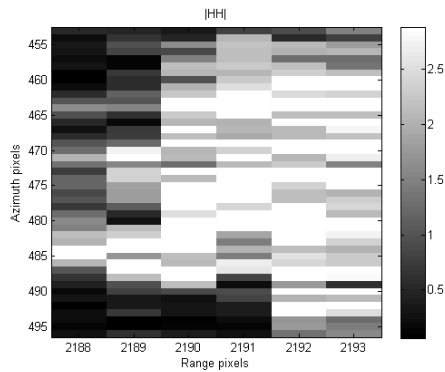
Figure 25: a) Detection performance for ship 9; b) $|HH|$ image and c) simulated $|X_1|$ image.

Original RADARSAT-2 Data and Products ©MacDonald, Dettwiler and Associates Ltd., 2008 – All Rights Reserved.

a)



b)



c)

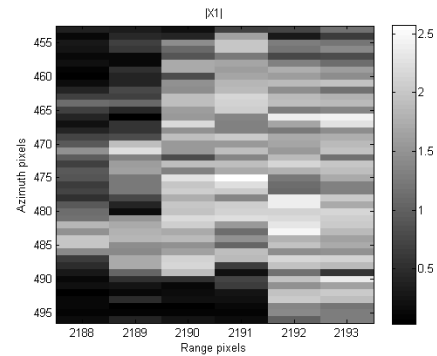


Figure 26: a) Detection performance for ship 10; b) $|HH|$ image and c) simulated $|X1|$ image.

Original RADARSAT-2 Data and Products ©MacDonald, Dettwiler and Associates Ltd., 2008 – All Rights Reserved.

List of acronyms

ADSS	Analysts' Detection Support System
AIS	Automatic Identification System
CFAR	Constant False Alarm Rate
CP	Compact Polarimetry
CL	Circular Transmit and Linear Receive
DND	Department of National Defence
DRDC	Defence Research & Development Canada
Dstl	Defence Science and Technology Laboratory (U.K.)
DSTO	Defence Science and Technology Organization (Australia)
EO	Electro-Optical
FAR	False Alarm Rate
FQ	Fine Quad Mode
GDAL	Geospatial Data Abstraction Library
GEOINT	Geospatial Intelligence
HH	Horizontal-Horizontal
HV	Horizontal-Vertical
IA Pro	Image Analyst Pro
IMO	International Maritime Organization
IR	Infrared
KCFAR	K-distribution Constant False Alarm Rate
LRT	Likelihood Ratio Test
MDA	MacDonald, Dettwiler and Associates Ltd
MMSI	Maritime Mobile Service Identification
MSSIS	Maritime Safety and Security Information System
NESZ	Noise Equivalent Signal Zero
PDF	Probability Density Function
P_{FA}	Probability of False Alarm
P_{MD}	Probability of Missed Detection
PolSAR	Polarimetric Synthetic Aperture Radar
PRF	Pulse Repetition Frequency

R&D	Research & Development
ROC	Receiver Operating Characteristic
SAR	Synthetic Aperture Radar
SLC	Single Look Complex
SOLAS	Safety of Life At Sea
SOTDMA	Self-Organized Time Domain Multiplex
VH	Vertical-Horizontal
VV	Vertical-Vertical
xml	eXtensible Markup Language

This page intentionally left blank.

DOCUMENT CONTROL DATA		
(Security classification of title, body of abstract and indexing annotation must be entered when the overall document is classified)		
1. ORIGINATOR (The name and address of the organization preparing the document. Organizations for whom the document was prepared, e.g. Centre sponsoring a contractor's report, or tasking agency, are entered in section 8.)	2. SECURITY CLASSIFICATION (Overall security classification of the document including special warning terms if applicable.)	
Defence R&D Canada – Ottawa 3701 Carling Avenue Ottawa, Ontario K1A 0Z4	UNCLASSIFIED	
3. TITLE (The complete document title as indicated on the title page. Its classification should be indicated by the appropriate abbreviation (S, C or U) in parentheses after the title.)		
Ship detection using RADARSAT-2 Fine Quad Mode and simulated compact polarimetry data		
4. AUTHORS (last name, followed by initials – ranks, titles, etc. not to be used)		
Liu, C., Vachon, P.W., English, R.A., and Sandirasegaram, N.		
5. DATE OF PUBLICATION (Month and year of publication of document.)	6a. NO. OF PAGES (Total containing information, including Annexes, Appendices, etc.)	6b. NO. OF REFS (Total cited in document.)
February 2010	68	22
7. DESCRIPTIVE NOTES (The category of the document, e.g. technical report, technical note or memorandum. If appropriate, enter the type of report, e.g. interim, progress, summary, annual or final. Give the inclusive dates when a specific reporting period is covered.)		
Technical Memorandum		
8. SPONSORING ACTIVITY (The name of the department project office or laboratory sponsoring the research and development – include address.)		
Defence R&D Canada – Ottawa 3701 Carling Avenue Ottawa, Ontario K1A 0Z4		
9a. PROJECT OR GRANT NO. (If appropriate, the applicable research and development project or grant number under which the document was written. Please specify whether project or grant.)	9b. CONTRACT NO. (If appropriate, the applicable number under which the document was written.)	
15el		
10a. ORIGINATOR'S DOCUMENT NUMBER (The official document number by which the document is identified by the originating activity. This number must be unique to this document.)	10b. OTHER DOCUMENT NO(s). (Any other numbers which may be assigned this document either by the originator or by the sponsor.)	
DRDC Ottawa TM 2009-285		
11. DOCUMENT AVAILABILITY (Any limitations on further dissemination of the document, other than those imposed by security classification.)		
unlimited		
12. DOCUMENT ANNOUNCEMENT (Any limitation to the bibliographic announcement of this document. This will normally correspond to the Document Availability (11). However, where further distribution (beyond the audience specified in (11) is possible, a wider announcement audience may be selected.)		
unlimited		

13. **ABSTRACT** (A brief and factual summary of the document. It may also appear elsewhere in the body of the document itself. It is highly desirable that the abstract of classified documents be unclassified. Each paragraph of the abstract shall begin with an indication of the security classification of the information in the paragraph (unless the document itself is unclassified) represented as (S), (C), (R), or (U). It is not necessary to include here abstracts in both official languages unless the text is bilingual.)

This Technical Memorandum presents an evaluation baseline for ship detection employing RADARSAT-2 Fine Quad (FQ) Mode imagery and an initial investigation of the potential performance for data obtained by a compact polarimetry (CP) SAR system. A CP SAR system with circular polarization on transmission and two orthogonal linear polarizations on receive was simulated using RADARSAT-2 FQ data. Polarimetric SAR (PolSAR) ship detection algorithms were applied to both the FQ and simulated CP data. From statistical decision theory, the likelihood ratio test with Neyman-Pearson criterion was used to define a decision variable.

FQ, dual polarization (including simulated CP, and horizontal polarization on transmit and horizontal and vertical polarizations on receive (HH + HV) with amplitude only), and single polarization (HH) images of known ships were considered. In this study, the smallest detected ship had a length of 18 m. The results demonstrate that a quad polarization system provides the best ship detection performance in this application as compared to single and dual polarization SAR systems. The results also demonstrate that a CP system provides better performance than a conventional dual polarization system and in turn than a single polarization system. It is important to note that CP, dual polarization and single polarization systems have a swath width that is twice as wide as that of a PolSAR having the same resolution.

Detection performance was characterized by calculating receiver operating characteristics for RADARSAT-2 FQ data and simulated CP data to quantify the trade-off between the probability of missed detection and the probability of false alarm. SAR detections were validated by using automatic identification system (AIS) data.

In further studies, detection algorithms based on the likelihood ratio test have been optimized and the decision variable defined using the likelihood ratio test has been input into a K-distribution constant false alarm rate (KCFAR) detector as the required image. The KCFAR PolSAR (KCFAR_Quad) detector found all targets for which AIS data were available, and also additional targets. Results show that this detector is capable of detecting smaller targets than those for a single polarization system.

14. **KEYWORDS, DESCRIPTORS or IDENTIFIERS** (Technically meaningful terms or short phrases that characterize a document and could be helpful in cataloguing the document. They should be selected so that no security classification is required. Identifiers, such as equipment model designation, trade name, military project code name, geographic location may also be included. If possible keywords should be selected from a published thesaurus, e.g. Thesaurus of Engineering and Scientific Terms (TEST) and that thesaurus identified. If it is not possible to select indexing terms which are Unclassified, the classification of each should be indicated as with the title.)

Synthetic aperture radar (SAR); polarimetric SAR; PolSAR; ship detection; compact polarimetry;

Defence R&D Canada

Canada's leader in Defence
and National Security
Science and Technology

R & D pour la défense Canada

Chef de file au Canada en matière
de science et de technologie pour
la défense et la sécurité nationale



www.drdc-rddc.gc.ca